Cement and Concrete Research 83 (2016) 1–18

Contents lists available at ScienceDirect

Cement and Concrete Research

journal homepage: www.elsevier.com/locate/cemconres

Hydration of water- and alkali-activated white Portland cement pastes and blends with low-calcium pulverized fuel ash

I.G. Richardson *, A.V. Girão [1], R. Taylor [2], S. Jia

School of Civil Engineering, University of Leeds, Leeds LS2 9JT, United Kingdom

ARTICLE INFO

Article history:
Received 20 August 2015
Accepted 22 January 2016
Available online xxxx

Keywords:
Calcium-silicate-hydrate (C-S-H)
TEM
Hydration
Fly ash
Retardation

ABSTRACT

Pastes of white Portland cement (wPc) and wPc-pulverized fuel ash (pfa) blends were studied up to 13 years. The reaction of wPc with water was initially retarded in the presence of pfa particles but accelerated at intermediate ages. Reaction with KOH solution was rapid with or without pfa. A universal compositional relationship exists for the C-A-S-H in blends of Pc with aluminosilicate-rich SCMs. The average length of aluminosilicate anions increased with age and increasing Al/Ca and Si/Ca; greater lengthening in the blends was due to additional Al^{3+} at bridging sites. The morphology of outer product C-A-S-H was always foil-like with KOH solution, regardless of chemical composition, but with water it had fibrillar morphology at high Ca/(Si + Al) ratios and foil-like morphology started to appear at Ca/(Si + Al) ≈1.2–1.3, which from the literature appears to coincide with changes in the pore solution. Foil-like morphology cannot be associated with entirely T-based structure.

1. Introduction

The main silicate phases that are present in Portland cement are a chemically impure tricalcium silicate (C_3S[3]) that is called alite, and an impure β-dicalcium silicate (β-C_2S) that is called belite [1]. The products of the hydration of these two phases are the same: a calcium silicate hydrate of variable composition and calcium hydroxide (CH), as shown in Eqs. (1) and (2) [2].

$$C_3S + (3 - x + y)H \rightarrow C_xSH_y + (3 - x)CH \quad (1)$$

$$C_2S + (2 - x + y)H \rightarrow C_xSH_y + (2 - x)CH \quad (2)$$

The values of x and y in Eqs (1) and (2) can vary and so the calcium silicate hydrate is commonly referred to as C-S-H, the dashes denoting non-stoichiometry. In neat C_3S pastes, the value of x – i.e. the molar Ca/Si ratio of the C-S-H – ranges between 1.3 and 2.1 [3] with a mean value of about 1.75 [4]. Substitution of this value for x into Eq. (1) and a value of 4.0 for y (which corresponds to a relative humidity (RH) of 90% [2]) shows that the mass % of calcium hydroxide in a fully reacted paste at 90% RH is 28.7%, or 40.6% when referred to the mass of the original C_3S (i.e. when expressed on the basis of the 'ignited weight'). The equivalent values for β-C_2S are 7.4 and 10.8%.

In addition to alite and belite, Portland cement also contains tricalcium aluminate (C_3A) and a calcium aluminoferrite phase, which is often represented as C_4AF although in a clinker it typically includes about 10% substituent oxides [5]. Whilst hydration of these phases results in the formation of calcium aluminate hydrates (AFt, AFm, hydrogarnet), some Al is also accommodated in the C-S-H; the Al/Si ratio is typically about 0.08 [3,6]. In concrete, Portland cement is often partially replaced by material that is either latently hydraulic (ground granulated blast-furnace slag (ggbs)) or pozzolanic (e.g. silica fume (sf), pulverized fuel ash (pfa), or metakaolin (mk)). Such materials are referred to as mineral admixtures, cementitious replacement materials (CRMs) or supplementary cementitious materials (SCMs). SCMs are a source of Al (except for sf) and Si during hydration but have either little or no Ca (the pozzolans) or a much-reduced amount (ggbs) when compared with Portland cement. The use of SCMs therefore results in C-S-H that has a lower Ca/Si ratio than occurs with neat Portland cement and – with the obvious exception of silica fume – in higher Al/Si ratio; Al-substituted C-S-H is often called C-A-S-H. The extent of the change in composition depends on the amount of SCM in the cement and on its degree of reaction. The most extensive set of compositional data for C-A-S-H in cement pastes that is demonstrably free of intermixture with other phases is for neat ordinary Portland cement (oPc) pastes or blends of oPc with ggbs: Richardson & Groves [6] collated TEM-EDX data from a number of studies on such systems [3,7,8] and showed that there is a good linear relationship between the Si/Ca and Al/Ca ratios, Eq. (3).

$$\frac{Si}{Ca} = 0.428 + 2.366\left(\frac{Al}{Ca}\right) \quad r^2 = 0.98 \quad (3)$$

* Corresponding author. Tel.: +44 113 3432331.
E-mail address: i.g.richardson@leeds.ac.uk (I.G. Richardson).
[1] Current address: Universidade de Aveiro, CICECO, 3810–193 Aveiro, Portugal.
[2] Current address: Department of Civil and Environmental Engineering, 760 Davis Hall, University of California, Berkeley 94720–1710, USA.
[3] C = CaO; S = SiO_2; A = Al_2O_3; H = H_2O.

http://dx.doi.org/10.1016/j.cemconres.2016.01.008

This linear relationship was confirmed by later work on older samples [9]. The change in the composition of the C-A-S-H is accompanied by a decrease in the quantity of calcium hydroxide [6,9,10] and a change in morphology of the C-A-S-H from fibrillar at low Si/Ca and Al/Ca ratios to foil-like at higher values [4,7,9].

Studies using trimethylsilylation-gel permeation chromatography (TMS-GPC; [11–14]) have indicated that the silicate anions that are present in the C-S-H that is formed in water-activated cements follow a 2, 5, 8, … (3*n*–1) sequence, where *n* is integer [15,16] and there is strong evidence that when Al^{3+} substitutes for Si^{4+}, the substitution only occurs in the central tetrahedron of pentameric linear chains, or in every third tetrahedron of longer chains [14,17–20]. These data support the view that the aluminosilicate anions that are present in C-A-S-H are linear chains that have the *Dreiereinfachketten* conformation [21] that is present in a number of natural calcium silicates, including 14 Å tobermorite [22], clinotobermorite 9 Å [23], pectolite [24–29], wollastonite [25,26,30–32], bustamite [30], hillebrandite [33], foshagite [34], and jennite [35]. The *Dreiereinfachketten* conformation involves infinite chains of tetrahedra that have a kinked pattern that has a 3-tetrahedron repeat sequence. In the tobermorite phases, pairs of silicate tetrahedra are clasped to a central Ca-O sheet (and so are called paired tetrahedra, abbreviated PT), and the gap between adjacent pairs is bridged by a single tetrahedron (which is called a bridging tetrahedron, BT). Removal of BT (i.e. the presence of vacant tetrahedral bridging sites) leads to the 2, 5, 8, … (3*n*–1) sequence of chain lengths that is observed in C-S-H. The two shortest chain segments are dimers and pentamers, which are shown schematically in Fig. 1 (reproduced from [36]); the unfilled triangles represent Si–O tetrahedra and the shaded triangle represents an Al–O tetrahedron. Whilst these are followed in the sequence by octamers, undecamers, etc., there is evidence that for semi-crystalline synthetic C-S-H preparations that have Ca/Si less than about 1.4, the anions are either dimeric or long-chain [37–44]. Richardson [36] has shown recently how this evidence can be accommodated through the interstratification of dimeric (T2) and infinite-chain (T∞) layers that were derived from the structure of a staggered-chain clinotobermorite. It is possible that a similar arrangement in also present in C-A-S-H that is less well-ordered, albeit with a greater fraction of vacant tetrahedral bridging sites in the T∞ layers and more stacking faults.

The mean length of the (alumino)silicate anions (called the mean chain length, MCL) can be calculated using Eq. (4) [45].

$$\mathrm{MCL} = \frac{2}{\left(\dfrac{Q^1}{Q^1 + Q^2(0Al) + \frac{3}{2}Q^2(1Al)}\right)} \tag{4}$$

In this equation – and those that follow – $Q^n(m\mathrm{Al})$ represents the relative intensity of a peak determined from the deconvolution of a ^{29}Si single-pulse MAS NMR spectrum (assuming that the spectrum was collected using quantitative conditions); there are 15 possible $Q^n(m\mathrm{Al})$ structural units where the silicate tetrahedron, Q, is connected via oxygen bridges to *m* Al and *n*-*m* other Si atoms, with $n = 0$ to 4 and $m = 0$ to *n* [46]. Andersen et al. [47] introduced a modified version of Eq. (4) that gives the mean length of just the silicate part of the chains, which can be written as Eq. (5):

$$\mathrm{MCL_{Si}} = \frac{2}{\left(\dfrac{Q^1 + Q^2(1\mathrm{Al})}{Q^1 + Q^2(0Al) + Q^2(1Al)}\right)} \tag{5}$$

The most extensive sets of MCL-composition data for C-A-S-H in hardened cements that incorporate SCMs are reported by Taylor et al. [8,48] for 20-year-old ggbs/oPc blends with full range of slag replacement (i.e. from 0 to 100%) reacted at normal temperature, and by Girão and co-workers [49,50] for 70% white Portland cement (wPc)–30% pfa pastes hydrated at elevated temperatures (55 and 85 °C) and aged up to 1 year. Those data show that the MCL lengthens with an increase in Si/Ca and Al/Ca ratios, with higher curing temperature, and with the age of the paste. The purpose of this paper is to supplement those data with additional data for blended cements that incorporate 30% pfa but reacted at 20–25 °C and aged for up to 13 years; for comparison, data are also included for pastes that contain 50% pfa aged for 9 and 13 years.

2. Experimental

Pastes of wPc and wPc blended with 30% low-calcium pfa were hand mixed with distilled water or with a 5 *M* KOH solution for 5 min in a plastic beaker. For the blended cement, the anhydrous wPc and pfa powders were first stirred together dry for 5 min and sieved to improve dispersion. All four systems were mixed at a liquid to solid ratio of 0.4 or 0.5 (mL g^{-1}) and were cast into 5 mL polystyrene specimen tubes, which were capped and heat sealed individually in polythene tubing: those at 0.4 were cured in a fog room at 20 ± 2 °C for 6, 10 and 15 h, 1, 3, 7, 14, 28 and 56 days; those at 0.5 were cured in a continuously stirred water bath at 25 ± 1 °C for 1 and 28 days, 1 and 4 years, and, in the case of the blended pastes, also for 9 and 13 years. Samples cured for 1 and 28 days were thus prepared using both liquid to solid ratios and curing conditions; the quantities of calcium hydroxide in the pastes at those ages were very similar ($\%CH_{L/S=0.5} = 1.03 \times \%CH_{L/S=0.4}$; $n = 8$; $r^2 = 0.97$) and so the data for the two liquid to solid ratios are as a consequence treated together and the CH data that are presented for these ages in §3 are average values. A water-activated blend with liquid to solid ratio of 0.5 was also made that contained 50% pfa, samples of which were examined after 9 and 13 years. Three batches of wPc and pfa were used in the work but they had very similar characteristics; the oxide composition for one of each obtained by X-ray fluorescence spectroscopy is given in Table 1. A small number of the blended samples were made with pfa from which magnetic particles had been removed using the following procedure: (i) the pfa was passed through a 75 μm sieve; (ii) the material was placed in a sealed plastic bag and a hand magnet (SEPOR Automagnet) used to isolate magnetic particles; (iii) the process was repeated until no more particles could be removed. The process had no impact on

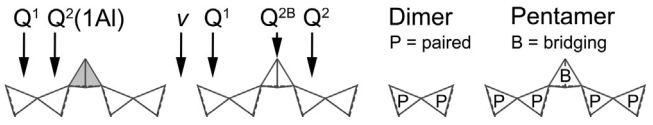

Fig. 1. Schematic diagram that illustrates the nature of the linear aluminosilicate chains that are present in C-S-H (reproduced from [36]). The $Q^n(m\mathrm{Al})$ notation is explained in the text following Eq. (4).

Table 1
Bulk oxide composition for the anhydrous wPc and pfa determined by XRF. The pfa included some mullite and quartz.

Oxide (mass %)	wPc	pfa
SiO_2	24.8	52.9
Al_2O_3	2.4	26.9
Fe_2O_3	0.5	8.6
MgO	0.8	1.7
CaO	68.6	4.5
SO_3	2.0	0.4
Na_2O	0.2	1.2
K_2O	0.1	3.3

the content of the major oxides other than a 13% reduction in iron oxide. The procedure was effective in reducing the paramagnetic line broadening of the peaks on ^{29}Si magic angle spinning (MAS) nuclear magnetic resonance (NMR) spectra. Comparison of thermal analysis data for samples prepared using pfa with and without magnetic particles indicated no significant differences and so the data are as a consequence treated together.

Most XRD measurements were performed using Panalytical X'PERT-PRO diffractometers (with X'Celerator real time multiple strip detector), operated with Cu Kα radiation at 40 mA and 40/45 kV. The samples were sliced using a slow-speed cut-off saw and mounted on a sample holder that was spun at 2 revolutions per second. XRD acquisition was carried out in continuous scan mode either over the range 6.03 to 54.95 °2θ with a step width of 0.01675° (i.e. 2921 steps) and a counting time of 34.29 s (corresponding to a total acquisition time of nearly 14 min), or 5.02 to 79.98 °2θ with a step size of 0.03342° (i.e. 2244 steps) and a counting time of 200.03 s (corresponding to a total acquisition time of nearly 61 min). XRD data were also collected using a Philips APD 1700 diffractometer (Cu Kα radiation; range 5 to 60° 2θ; scan speed of 0.025° s^{-1}; step size of 0.05°).

The quantity of calcium hydroxide in the pastes was determined by thermogravimetry (STA1500, Stanton Redcroft, London, UK) using the 'tangent' analysis method to account for the mass loss associated with the concurrent dehydration of other phases [51–53]. The hydration of early-age samples was quenched using propan-2-ol followed by vacuum outgassing; samples were crushed and ground to a powder in an agate mortar, and were heated under a constant flow of nitrogen to 1000 °C at 20 °C/min; values for % calcium hydroxide are given in terms of the residual mass at 1000 °C (i.e. the 'ignited weight'). An evolved gas analysis (EGA) system (Cirrus mass spectrometer, MKS Spectra Products Ltd., UK) was interfaced with the STA equipment for many of the sample runs to differentiate mass loss associated with water or carbon dioxide: in fact, CO_2 was not detected in any of those samples thus confirming that no carbonation occurred during storage or sample preparation.

The cumulative heat evolved during early hydration was measured using a JAF isothermal conduction calorimeter (Wexham Developments, Reading, Berkshire, UK; 25 °C; water to solid ratio of 0.5 (mL g^{-1})) with external mixing [54,55]).

Solid-state ^{29}Si single-pulse MAS NMR spectra were acquired using a Varian InfinityPlus 300 spectrometer (magnetic field 7.05 T; operating frequency of 59.5 MHz for ^{29}Si). Samples for NMR were freshly ground to a powder in an agate mortar, packed into 6 mm zirconia rotors sealed at either end with Teflon end plugs, and spun at 6 kHz in a Chemagnetics-style probe. The spectra were acquired for between 5760 and 27,616 scans using a pulse recycle delay of 2 or 5 s, a pulse width 2 or 4 μs, and an acquisition time of 20 ms. ^{29}Si chemical shifts were referenced to tetramethylsilane (TMS) at 0 ppm, with kaolinite used as an external standard at −91.2 ppm. Quantitative information on the fractions of Si present in silicate tetrahedra with different connectivities was obtained by deconvolution of the single-pulse spectra. In this work, the spectra were fitted using a procedure that involves the subtraction of a contribution from a spectrum taken from anhydrous cement, which thus accounted for the unreacted alite and some of the belite, followed by the iterative fitting of peaks for the remaining belite, pfa and C-A-S-H peaks to Voigt line shapes [49,56]. As in previous work [49,50] it was found that it was not possible to quantify the extent of reaction of the glassy pfa because for the pfa (but not the other peaks) the ratio of the signal in the centre band to that in the sidebands varied unpredictably with age; further work is required to determine the reasons for this. ^{27}Al MAS NMR spectra were collected (magnetic field 9.4 T; operating frequency of 104.2 MHz for ^{27}Al) using a pulse recycle delay of 0.2 s, a pulse width of 1.0 μs and an acquisition time of 10 ms, for 10,000 repetitions. The ^{27}Al chemical shifts are given with respect to 1 *M* $[Al(H_2O)_6]^{3+}$ as an external standard, and are not corrected for second order quadrupolar effects. The samples were spun for no longer than 40 min in order to avoid dehydration of the sample and any consequent loss in intensity of peaks [57].

Transmission electron microscopy with energy dispersive X-ray analysis (TEM-EDX) was used to examine the morphology of the C-A-S-H and to determine its chemical composition (Philips CM20, Eindhoven, Netherlands, equipped with an UTW EDX detector, Oxford, UK, and ISIS software for imaging/X-ray analysis, Oxford Instruments). The microscope was operated at 200 kV. For TEM, 200 μm-thick slices were hand thinned, using silicon carbide paper of different grades (600–2400 grit from Struers, Glasgow, UK), until they were approximately 30 μm thick. Ni or Cu grids with a 2 × 1 mm slot were glued onto both sides of the sample as a 'sandwich'. The specimens were then argon ion-beam milled (Model 1010 Ion Mill, Fischione Instruments, PA, U.S.A.) using a liquid nitrogen cooled stage in order to avoid excessive specimen heating and consequent damage/alteration. The specimens were carbon coated after milling. Between 30 and 76 regions of C-A-S-H were analysed – including both inner (Ip) and outer product (Op) C-A-S-H – which were taken randomly around the thinner areas of the samples. Each region was checked before EDX analysis by selected area electron diffraction (SAED) for the presence of crystalline phases. This strategy ensured that in the water-activated samples analyses were obtained of C-A-S-H free of intermixture with other phases, except the AFt-type phase, which is sufficiently unstable under the electron beam that it loses structural order and consequently gives no crystalline reflections (i.e. spots) on the electron diffraction pattern; mixtures of C-A-S-H with the AFt-type phase were therefore identified on the basis morphology and compositional trends and such analyses were excluded when calculating mean compositions for C-A-S-H. Both XRD and TEM-SAED indicate that KOH-activation results in CH that is microcrystalline, and imaging in the TEM reveals microcrystals of CH intimately mixed on a nanometre scale with layers of semi-crystalline C-S-H(I) [6,58]. This fine-scale mixing presents a problem when attempting to determine the composition of C-S-H that is free of intermixture with other phases; this issue is discussed further in §3.2.

3. Results and discussion

3.1. Phases present in the hardened pastes

The XRD showed that the crystalline phases present in the water-activated neat cement paste included unreacted alite and belite, CH and AFt; the blended cement pastes contained the same phases together with some mullite and quartz from the pfa. Residual cement phases were present at all ages, although only belite in the older samples. AFt was not present in the KOH-activated pastes and the CH peaks were broad, indicating a small average crystal size; a trace amount of hydrogarnet appeared at later age in the KOH-activated blend. These data are consistent with work on synthetic cements (blends of C_3S, C_3A and gypsum) where the preferred phases for hydration in water were C-S-H, CH and ettringite but only C-S-H and CH for hydration in KOH solution, with the C-S-H containing sulphate and aluminate ions [59]. Whilst AFm-type phases were not detected by XRD in any of the systems studied in this work, a peak assigned to $Al^{[6]}$ in AFm is present on the ^{27}Al NMR spectra for the water- and KOH-activated pastes, as illustrated in Fig. 2 for the 9-year-old pastes (i.e. the peak at a chemical shift of ≈9 ppm; [60,61]); presumably there was either too little AFm in the pastes or the crystals were not sufficiently large or ordered to be detected by XRD. Peaks are also present on the ^{27}Al NMR spectra for both methods of activation at ≈5 ppm, ≈35 ppm and ≈62 ppm. The peak at ≈5 ppm is assigned to the 'third aluminate hydrate' (TAH) [61]; Andersen et al. [61] proposed that TAH is either an amorphous/disordered aluminate hydroxide or a calcium aluminate hydrate, formed as a separate phase, possibly as a surface precipitate on the C-S-H. The peak at ≈35 ppm is assigned to Al in fivefold coordination that has been attributed to AlO_5 sites in the interlayer of the C-A-S-H [20,61,62]. The peak at ≈62 ppm is assigned to Al in fourfold

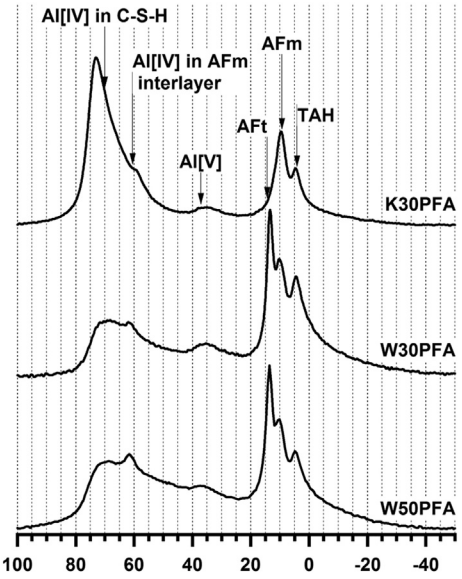

Fig. 2. ^{27}Al MAS NMR spectra for 9-year-old water-activated pastes with 30% and 50% pfa and for a KOH-activated paste with 30% pfa. The spinning speed was 12 kHz and the most intense peak for each spectrum is set to the same height.

coordination that is possibly due to the presence of an aluminosilicate anion in the interlayer of the AFm phase. This is supported by recent results for metakaolin-wPc pastes in which a peak at 61 ppm was attributed to a very small amount of strätlingite, ^{27}Al NMR being more sensitive to the detection of strätlingite than powder XRD [62]. The peak at ≈13 ppm on the spectra for water-activated pastes is assigned to AFt [60,61].

3.2. Evolution of $Ca(OH)_2$ content

The filled circle symbols on the lower part of Fig. 3(a) show the quantity of CH in the water-activated paste that contains 30% pfa expressed as a percentage of ignited mass. For comparison, the unfilled circles indicate the values that were measured for the neat cement paste multiplied by 0.7; the unfilled circles therefore represent the quantities of CH that might be expected in the blend on the basis of simple dilution. The top half of the figure shows the result of dividing the values measured for the blend by those for the neat cement multiplied by 0.7, referred to here as $CH^{actual}/CH^{expected}$: a value <1 means that there was less CH than expected on the basis of simple dilution and a value >1 means that there was more than expected. Fig. 3(b) shows the same information as (a) but for the KOH-activated pastes.

The top part of Fig. 3(a) shows that for the first few days of hydration the 'expected' quantity of CH in the water-activated blend is greater than the observed quantity (i.e. $CH^{actual}/CH^{expected} < 1$), and this observation is supported by the fact that the cumulative heat evolution curve for the blend is lower than the curve for the neat cement multiplied by 0.7 i.e. less heat was evolved in the blend than expected on the basis of dilution; the cumulative heat evolution curves are presented in Fig. 4(a) (bottom part, left-hand axis) together with CH data (top, right-hand axis). The CH and heat evolution data both indicate that the hydration of the cement was initially retarded in the presence of the pfa particles. This is the opposite of a view that seems to be becoming widely held (e.g. [63,64]) that the hydration of the Portland cement in blends that contain pfa is always initially accelerated i.e. that the hydration is consistent with the so-called 'filler effect' (the 'filler effect' has been studied and discussed extensively e.g. [63,65–70]). This view has perhaps emerged because the earliest age at which the quantity of CH was determined in a lot of studies is 1 day or later (e.g. [53,71–82]), when the value of $CH^{actual}/CH^{expected}$ is generally greater than 1, thus indicating that there is more CH than expected. However, it has long been recognized that the effect of pfa particles on the early hydration of the Portland cement is variable and complex (e.g. [83,84]). As an example, this variability is starkly evident when comparing just a few studies that were published in the early 1980s: the aluminate reaction in Portland cement was considered by Plowman and Cabrera [85,86] to be retarded, but accelerated by Uchikawa & Uchida [87]; the silicate reaction was considered by Ogawa et al. [88] to be accelerated, but retarded by Jawed & Skalny

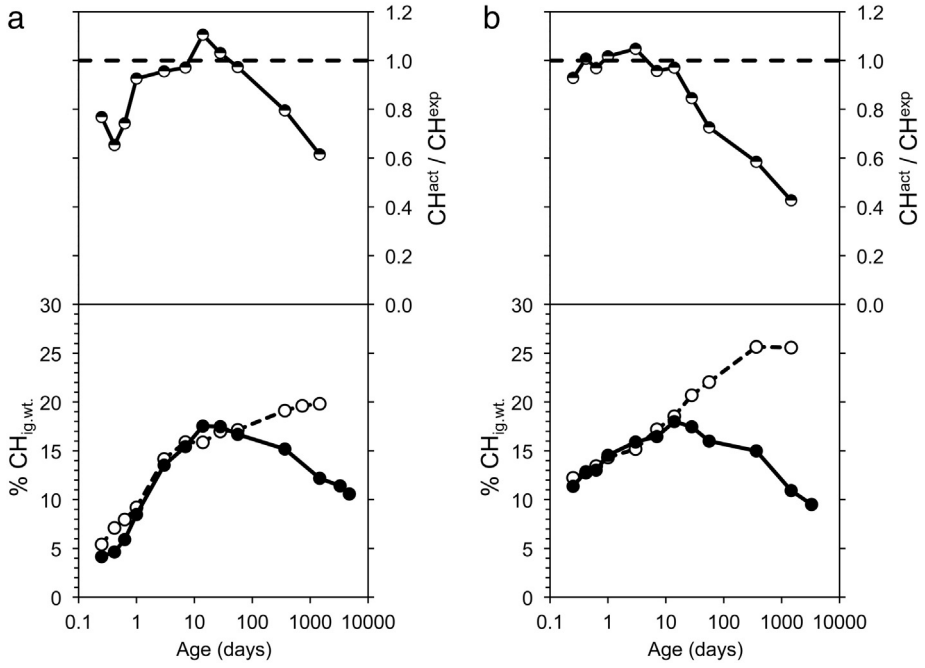

Fig. 3. (a) The bottom half of the figure shows the variation in % CH (ig. wt.) with age for the water-activated neat wPc (open circles) and the blend with 30% fly ash. The data for the neat cement are multiplied by 0.7 to facilitate comparison with those for the blend, the former thus representing the quantities of CH that might be expected in the blend on the basis of simple dilution. The top half of the figure shows the result of dividing the values measured for the blend by those for the neat cement multiplied by 0.7, referred to as $CH^{actual}/CH^{expected}$. Fig. 3(b). The same as (a) but for the KOH-activated pastes.

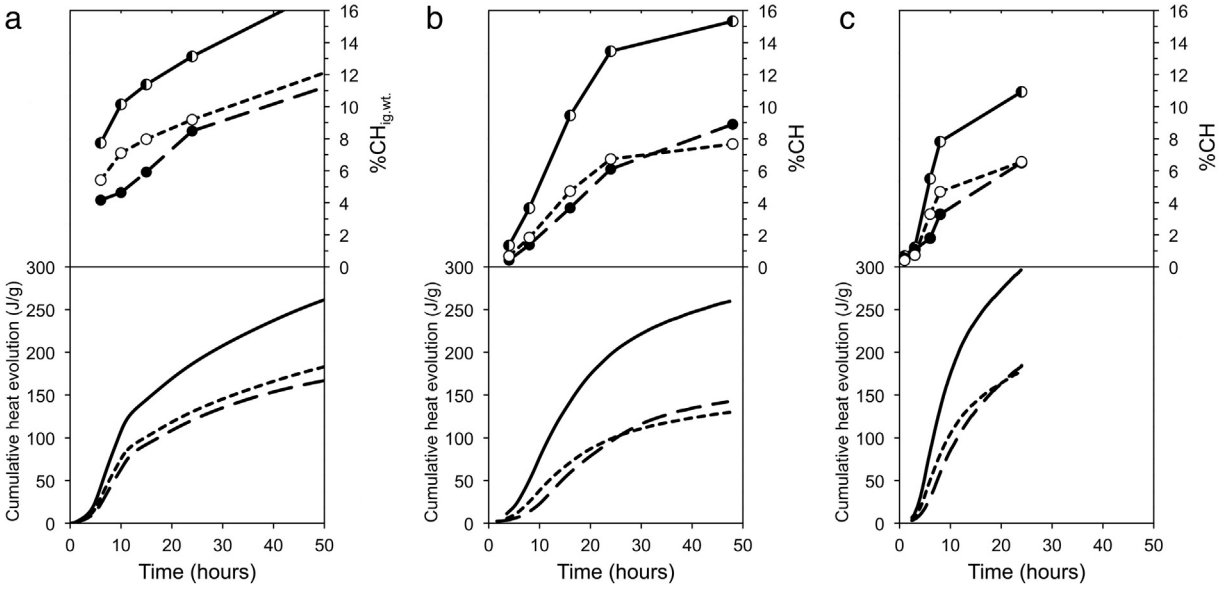

Fig. 4. (a) Variation in the cumulative heat evolved (lines) and % CH formed (circles) over the first 2 days hydration for the water-activated pastes. The cumulative heat evolution curves refer to the left-hand axis and the % CH (ig. wt.) refer to the right-hand axis. Data for the neat wPc are represented by the full line and half-filled circles; the values for neat wPc × 0.7 are represented by the short-dashed line and unfilled circles; and those for the 70% wPc-30% pfa paste by the long-dashed line and filled circles. Equivalent data from [92] (48 h) and [83] (24 h) are shown in (b) and (c) respectively. It should be noted that the absolute values of %CH shown in the three parts of this figure cannot be compared directly with one another because [83,92] do not appear to have allowed for the concurrent dehydration of other phases; the values from [92] are expressed in terms of the residual mass at 500 °C rather than 1000 °C, and Fajun et al. [83] do not state the basis of their values.

[89] and Halse et al. [90]; and Ghose & Pratt [91] considered the silicate and aluminate reactions to both be retarded. These apparently contradictory results are due to the fact that the rates at which the various phases react in pfa-cement blends depend on many factors, which include: the chemical composition and physical characteristics of both the pfa and Portland cement (and if the cement fraction consists of synthesized phases instead of Portland cement); the pfa:cement ratio; the compositional heterogeneity of the glassy phase in the pfa; the temperature of hydration; and the water:solids ratio.

Conduction calorimetry and %CH data from two other studies ([83, 92]) that also demonstrate early-age retardation are compared directly with the data from this work in Fig. 4. It is evident that in all three studies the heat evolved from the blend was initially less than 'expected' and that the relative positions of the heat evolution curves are mirrored in all cases by the plots for %CH. The values of $CH^{actual}/CH^{expected}$ are thus <1 at early ages, consistent with the initial retardation of the hydration of the cement fraction; this is illustrated in Fig. 5, which is a compilation of some relevant data from the literature together with the data from this work (the sources of the data are given in the figure caption). Nevertheless, it is also clear from this figure that the value of $CH^{actual}/CH^{expected}$ does rise above 1 in most studies at intermediate ages, which must be due to acceleration of the cement hydration (i.e. consistent with the 'filler effect'), and then subsequently falls below 1 because of the consumption of CH by the pozzolanic reaction of the glassy phase in the pfa. In this study, the value of $CH^{actual}/CH^{expected}$ peaked at 14 days, and then dropped steadily with continued hydration. Comparison with the other studies shows that there is considerable variation in the age at which the measured value of CH dropped below the 'expected' value, which is indicative of variations in the behaviour of different ashes and cements. As examples, it occurred between 3 and 7 days in [93], at 1 week in [96], 1–2 weeks in [53,92], at about 2 months in [77], and at about 3 months in [80]. The value measured in this work at 4 years is much lower than the 'expected' value and the reducing trend for the measured value of CH continues at 9 and 13 years (see lower part of Fig. 3(a)), which shows that the glassy part of pfa continues to react over extended periods of time.

The lower part of Fig. 3(b) shows the variation in CH content with age for pastes activated with the 5 *M* KOH solution. The filled symbols again represent the data for the blend (i.e. with 30% pfa) and the open symbols represent the data for the neat alkali-activated cement paste multiplied by 0.7, i.e. again, the values that might be expected on the basis of simple dilution. Comparison of the two values at early age with those on Fig. 3(a) for water activation shows very clearly the acceleratory effect of the very high concentration of hydroxyl ions in the alkali-activated paste: more than twice the amount of CH was present at 6 h hydration with alkali activation than with water. In contrast to

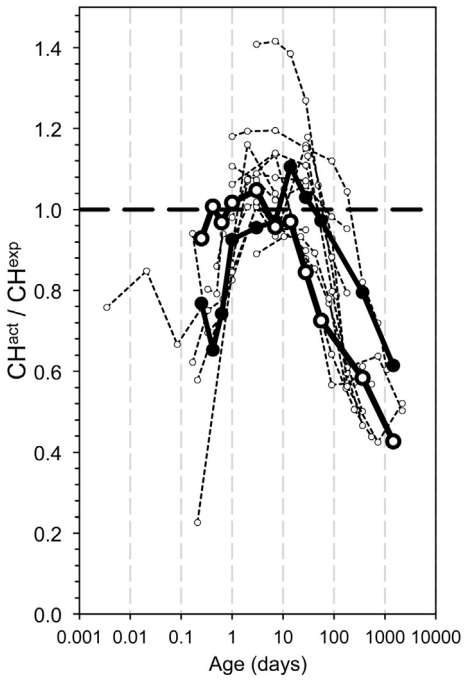

Fig. 5. $CH^{actual}/CH^{expected}$ data for both the water-activated pastes (filled circle) and KOH-activated (large open circles) replotted from Fig. 3 with data from the literature (small filled circles; individual data sets joined by dotted lines; data from [53,72,74,75,79,81,92–95].

the water-activated pastes, the values measured for the KOH-activated blend were very similar at early ages to those that might be 'expected' on the basis of dilution, indicating that the reaction of the cement fraction was not affected by the presence of the pfa particles (it was rapid with or without pfa). Reaction of the glassy part of the pfa is evident at intermediate and extended ages by the reduction in the quantity of CH.

3.3. Chemical composition of C-A-S-H

It is noted in §1 that both XRD and TEM-SAED indicate that KOH-activation results in CH that is microcrystalline, and that imaging in the TEM reveals microcrystals of CH that are intimately mixed on a nanometre scale with layers of semi-crystalline C-S-H(I) [6,58].This fine-scale intermixture means that the maximum Ca/Si ratio of the C-A-S-H is quite difficult to establish because a number of layers of CH-like structure could be interstratified with those of the C-A-S-H before rings for CH would be evident on the electron diffraction pattern; a possible topotactic relationship between CH and C-S-H(I) has been demonstrated recently that could explain how this fine-scale intermixture occurs [36]. It follows from this that for alkali-activated systems it is perhaps best to consider that high Ca/Si analyses from regions ostensibly of C-A-S-H and lacking CH diffraction rings are due to a low (≤ 1.5) Ca/Si ratio C-A-S-H that is interstratified with CH i.e. as envisaged in Richardson & Groves' T/CH structural viewpoint [16], which is discussed further below.

Fig. 6(a) and (b) shows the variation with age from 28 days of the mean Ca/Si and Al/Si atom ratios of the C-A-S-H (both Op and Ip) in the neat (open circle) and blended (30% pfa) cements for activation with water (Fig. 6(a)) and KOH solution (Fig. 6(b)). The mean Ca/Si of the C-A-S-H in the neat Portland cement pastes was higher with activation with water than with KOH solution, which is consistent with the greater quantity of CH measured in the latter (see Fig. 3). The Ca/Si ratio of the C-A-S-H was lower in the water-activated blend (filled circles) than in the neat paste (unfilled circles) (lower part, left-hand axis of Fig. 6(a)) and the Al/Si ratio was higher (upper part, right-hand axis of Fig. 6(a)), both of which are consistent with the reaction of some of the glassy pfa. Partially reacted pfa particles were observed at all ages examined by TEM, including at 28 days (the youngest sample examined by TEM-EDX): as examples, partially reacted pfa particles are shown in Figs. 7 and 8, which are respectively bright-field TEM images of regions in the water-activated pastes with 30% pfa hydrated for 4 years and with 50% pfa hydrated for 9 years. The conclusion must be that a quite significant fraction of the pfa had reacted by 28 days and that the presence of the pfa had also resulted in accelerated reaction of the cement fraction by this age (as discussed in §3.2), which is supported by the CH data in Fig. 3 and also by semi-quantitative analysis of the XRD patterns: comparison of the integrated intensity of the alite peak at around 51.5° 2θ (Cu Kα radiation) for the blend with that for the neat cement paste indicates that the quantity of alite that would be expected on the basis of simple dilution is present in the blend at 1 day but the quantity at 28 days was less than expected (the

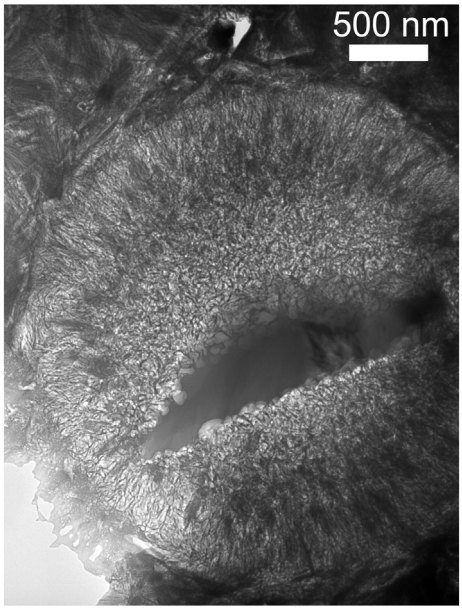

Fig. 7. TEM micrograph of Ip C-A-S-H and residual glassy phase in a partially reacted pfa particle in the water-activated wPc-30% pfa paste reacted for 4 years.

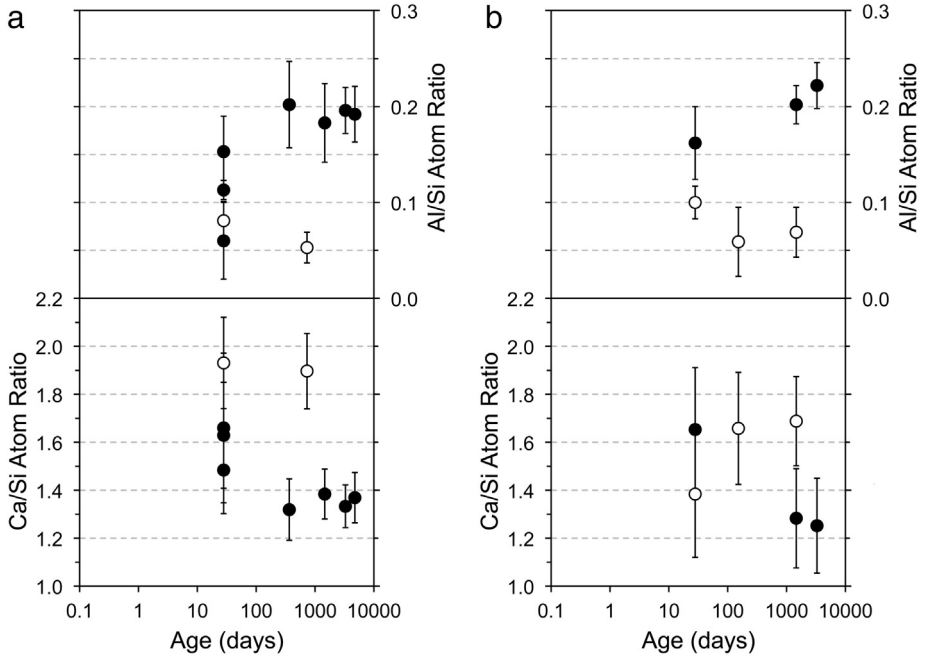

Fig. 6. (a) Variation with age of the mean Ca/Si (bottom) and Al/Si atom ratios of C-A-S-H (both Op and Ip) in neat water-activated wPc (open circle) and 70% wPc-30% pfa pastes determined by TEM-EDX. Error bars = 1 standard deviation. (b) The same but for the KOH-activated pastes.

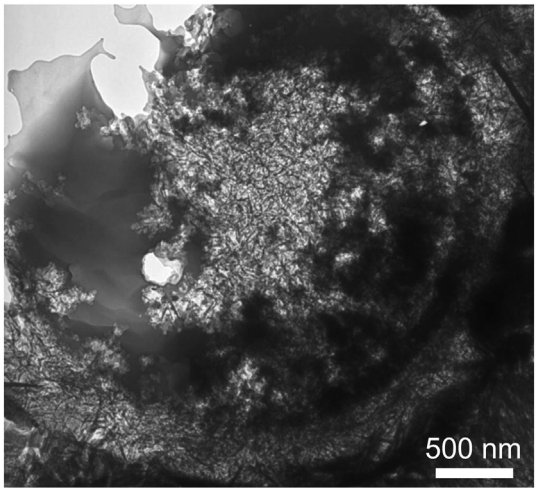

Fig. 8. TEM micrograph of Ip C-A-S-H and residual glassy phase in a partially reacted pfa particle in the water-activated wPc-50% pfa paste reacted for 9 years.

ratio of actual: 'expected' alite = 1.0 at 1 day but 0.5 at 28 days). As noted above, reaction of the glassy part of the pfa is evident at intermediate and extended ages in the KOH-activated blends by the reduction in the quantity of CH, and this is supported by imaging in the TEM (e.g. the large micrograph in Fig. 9 shows a reacted pfa particle in the KOH-activated paste with 30% pfa hydrated for 4 years), and by the decrease in the mean Ca/Si ratio of the C-A-S-H and increase in its mean Al/Si ratio (Fig. 6(b)). The anomalous Ca/Si values for the C-A-S-H in the 28-day-old pastes is possibly due to the difficulty in excluding calcium hydroxide from the TEM-EDX analyses, as noted above.

Fig. 10 is a plot of mean Al/Ca ratio against Si/Ca ratio for outer product C-A-S-H that is present in water-activated neat cement pastes or pastes with 30 or 50% of the cement replaced by pfa, hydrated at 25 °C (filled circles; data from this work and [97]), 55 °C (half-filled circles; data from [50,98]), or 85 °C (unfilled circles; data from [49]). There is a good linear relationship between the two ratios with the linear regression equation:

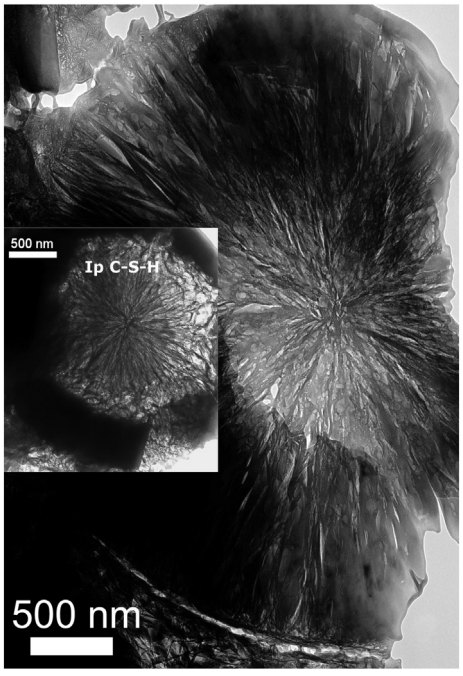

Fig. 9. TEM micrograph of Ip C-S-H in a fully reacted pfa particle in the KOH-activated wPc-30% pfa paste hydrated for 4 years. The inset micrograph shows Ip C-A-S-H that has similar spoke-like linear morphology in the water-activated wPc-30% pfa paste reacted for 1 year.

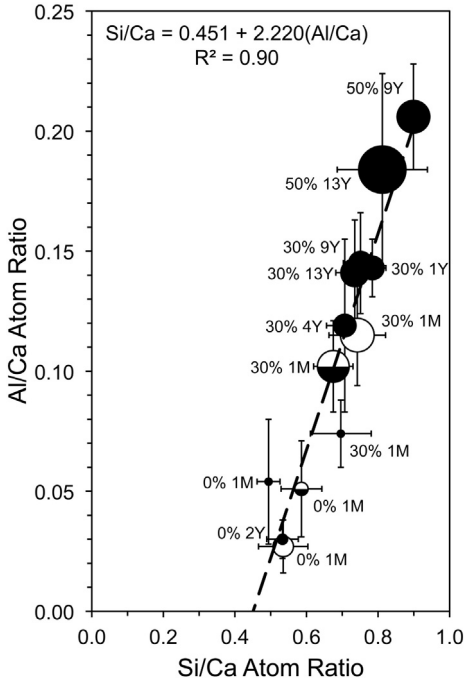

Fig. 10. Plot of the mean Al/Ca ratio against Si/Ca ratio for outer product C-A-S-H present in the water-activated hardened cement pastes measured directly in the TEM (by EDX; just Op to enable direct comparison with data for ggbs-PC blends [6]). The figure includes data for the C-A-S-H in the following systems: wPc pastes aged 28 days and 2 years; wPc-30% pfa pastes aged 28 days, 1 year, 4, 9, and 13 years; wPc-50% pfa paste aged 9 and 13 years. In addition, the plot includes data for 28-day-old samples of neat wPc and wPc-30% pfa pastes hydrated at 55 °C (half-filled symbols; [50,98]) and 85 °C (unfilled symbols; [49]). The error bars correspond to 1 standard deviation. The diameter of the symbols is proportional to the MCL.

$$\frac{Si}{Ca} = 0.451 + 2.220\left(\frac{Al}{Ca}\right) \quad r^2 = 0.90 \tag{6}$$

Eq. (6) is very similar to the equation reported in [6] that was established using data from a number of studies on cement pastes that incorporate ground granulated blast-furnace slag (ggbs; [8,16,17]), i.e. Eq. (3). The similarity between these equations suggests strongly that this compositional relationship is universal for the C-A-S-H that is present in cement blends that incorporate aluminosilicate-rich supplementary cementitious materials. Comparison with data for synthetic preparations of C-A-S-H(I) (a semi-crystalline tobermorite-like phase that is often used as a model for the C-A-S-H that forms in cements) indicates that the amount of Al that is incorporated into the C-A-S-H in cements is likely to be a practical maximum, and that the synthetic preparations of most studies cannot be taken to represent the C-A-S-H in real cements because the compositions are generally not similar [36], a conclusion that also applies to a recent study [99].

3.4. Assignment of the peak on ^{29}Si MAS NMR spectra at ≈−82 ppm to Q^2(1Al)

^{29}Si MAS NMR has for many years been used to probe the structure of the C-A-S-H that is present in hardened cements and it can provide quantitative information on the fractions of silicon present in different tetrahedral environments, $Q^n(m\text{Al})$, as noted in §1. Increased polymerization of the Q^n tetrahedra causes characteristic up-field chemical shifts [46], and early studies on C_3S pastes showed that peaks at about −79

and −85 ppm were due respectively to end- (Q^1) and middle-chain (Q^2) groups in linear silicate chains present in C-S-H [100–105]. In aluminosilicates the shifts are further influenced by the replacement of Si by Al in tetrahedra adjacent to a given Si site, generally producing down-field shifts of ≈3 to 5 ppm per Al [46]. The nature of the aluminosilicate chains that are present in C-A-S-H are illustrated in Fig. 1. Consistent with the above, Richardson et al. [18] assigned the peaks at around −79, −82 and −85 ppm on the SP MAS ^{29}Si NMR spectrum for an alkali-activated synthetic slag-glass paste to Q^1, Q^2(1Al) and Q^2(0Al) in C-A-S-H. The Al/Si ratio of the C-A-S-H was calculated from the NMR data using Eq. (7) [45] and the result was in excellent agreement with the value measured directly by analytical TEM.

$$\mathrm{Al/Si} = \frac{\frac{1}{2}Q^2(1Al)}{Q^1 + Q^2(0Al) + Q^2(1Al)} \tag{7}$$

Richardson et al. [18] concluded that the Al atoms in the C-A-S-H must have substituted for Si only in the central tetrahedron of pentameric linear chains – i.e. in the bridging tetrahedron – because no peak that corresponded to Q^1(1Al) units was observed on the ^{1}H-^{29}Si cross polarization (CP) MAS NMR spectrum. If, assuming the absence of chain-terminating Al, Al substituted for Si at tetrahedral sites other than in bridging tetrahedra, then Q^1(1Al) units would be expected to be present; a significant number of chain terminating Al could not have been present because that would have resulted in a higher Al/Si ratio calculated by NMR than that derived from TEM-EDX analysis, which was not observed. The same situation was later shown to exist for a range of slag-containing cements [14] and it is also the case for the neat cement and pfa blends studied in this work. This is evident from Fig. 11, which is a plot of the Al/Si ratio of the C-A-S-H measured directly in the TEM compared with the value calculated from the results of the deconvolution of the single-pulse ^{29}Si NMR spectra using Eq. (7), with the peak at ≈−82 ppm assigned entirely to Q^2(1Al). As an example of the results of the deconvolution of the ^{29}Si NMR spectra, the spectrum for the paste with 50% pfa aged for 9 years is shown in Fig. 12; the Al/Si ratio of the C-A-S-H in that paste – calculated from the results of the deconvolution of the spectrum using Eq. (7) – is 0.22, which is in excellent agreement with the mean value determined directly by TEM-EDX i.e. 0.22 ± 0.02 (n = 36). Fig. 11 and the regression analysis equation, Eq. (8), show that in general the two techniques give very similar values, which provides confidence in the deconvolution procedure and the assignment of the peak at ≈−82 ppm to Q^2(1Al).

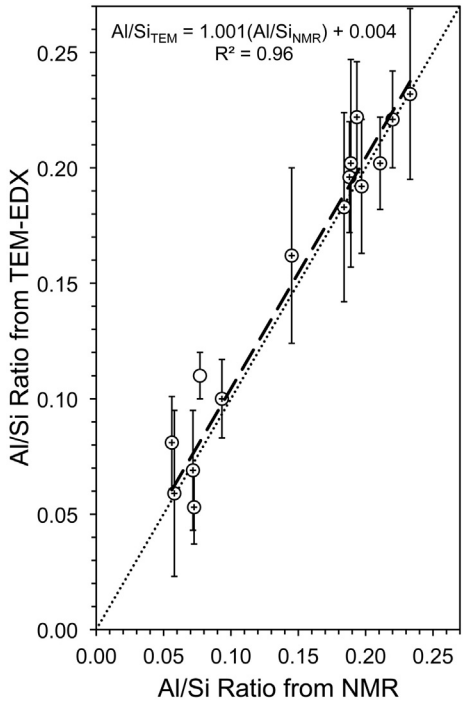

Fig. 11. Plot of the average Al/Si ratio of the C-A-S-H present in the hardened cement pastes measured directly in the TEM (by EDX; including analyses of both Op and Ip C-A-S-H) compared with the value calculated from the deconvolution of the single-pulse ^{29}Si NMR spectrum. The figure includes data for the C-A-S-H in the following systems: water-activated neat wPc pastes aged 28 days and 2 years; water-activated wPc-30% pfa pastes aged 28 days, 1 year, 4, 9, and 13 years; alkali-activated neat wPc pastes aged 28 days, 5 months, and 4 years; alkali-activated wPc-30% pfa pastes aged 28 days, 4 years, and 9 years; water-activated wPc-50% pfa paste aged 9 and 13 years. The error bars for the TEM-EDX data correspond to 1 standard deviation. Data used for the regression analysis are indicated using a '+' inside the circle symbol, which includes all but one of the data points (the anomalous point for the water-activated 28-day-old blend was excluded from the analysis).

$$\left(\frac{\mathrm{Al}}{\mathrm{Si}}\right)_{\mathrm{TEM}} = 0.004 + 1.001\left(\frac{\mathrm{Al}}{\mathrm{Si}}\right)_{\mathrm{NMR}} \quad r^2 = 0.96 \tag{8}$$

3.5. ^{29}Si MAS NMR

The results from the deconvolution of the ^{29}Si MAS NMR spectra are shown in Figs. 13 to 17. Fig. 13 shows how the extent of hydration of the silicate phases (alite + belite) in neat white Portland cement pastes varied with age for activation by water (open circles) or KOH solution (filled circles). The % hydration was much greater at 1 day with KOH than with water (about 47% compared with 36%; indicated by the bold arrow), which is consistent with the much higher % CH (Fig. 3). Acceleration of the reaction by KOH solution has been reported previously for C_3S pastes [107]. The extent of reaction at later ages was essentially the same regardless of the method of activation and it is notable that the data for the water-activated paste are very similar to those reported by Andersen et al. [47] and Sáez del Bosque et al. [106]; i.e. the reaction kinetics are very similar in the three studies.

Fig. 14 shows the % Si present as Q^0 (alite plus belite; diamond), Q^1 (circle), Q^2(1Al) (triangle) and Q^2(0Al) (square) plotted against age for activation with water (open symbols) and KOH solution (filled symbols). The data for the hydrate peaks are normalized in Fig. 15(a), thus indicating more clearly how the proportions of the different silicate species in the C-A-S-H varied with age. It is evident that the early-age

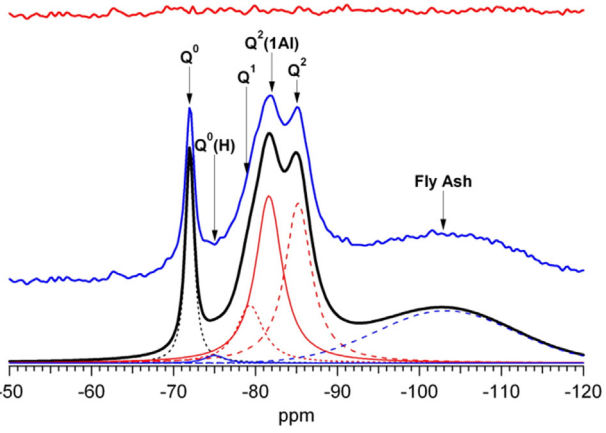

Fig. 12. Single-pulse ^{29}Si MAS NMR spectrum (middle) for a water-activated 50% wPc-50% pfa blend hydrated for 9 years at 25 °C. The result of the deconvolution of the spectrum is shown at the bottom and the residual at the top. The C-A-S-H peaks have chemical shifts of −79.3 for Q^1, −81.6 for Q^2(1Al), and −85.2 for Q^2(0Al); there is a small Q^{0H} peak at −75.0 ppm. The spectrum was acquired over 5760 scans using a pulse recycle delay of 5 s, a pulse width of 6 μs and an acquisition time of 20.5 ms.

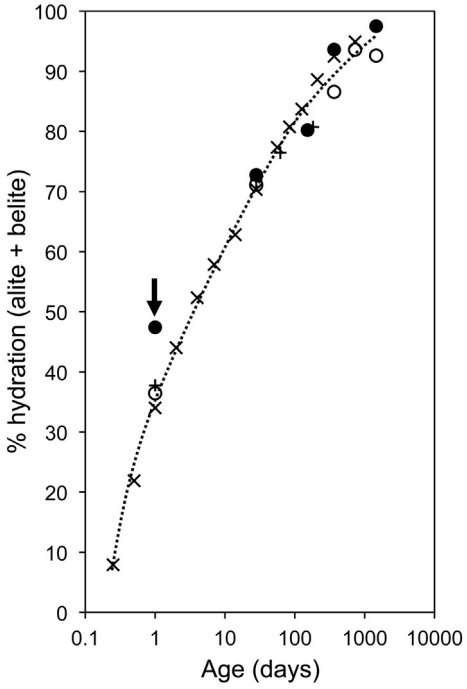

Fig. 13. Plot of % hydration against age for the neat white Portland cement activated by water (open circles) or KOH solution (filled circles). Data for water-activated neat white Portland cement pastes are also included from [47] (×; w/c = 0.5; 20 °C) and from [106] (+; w/c = 0.425; 25 °C). The dotted line is a guide for the eye.

C-A-S-H was dominated by Q^1, which is consistent with observations of the predominance of dimer at early age (e.g. [13] for alite pastes). The fraction of Q^1 decreased significantly with age, accompanied by increased $Q^2(0Al)$ and only limited variation in the fraction of $Q^2(1Al)$ (between about 1 in 10 and 1 in 7), which corresponds to a longer

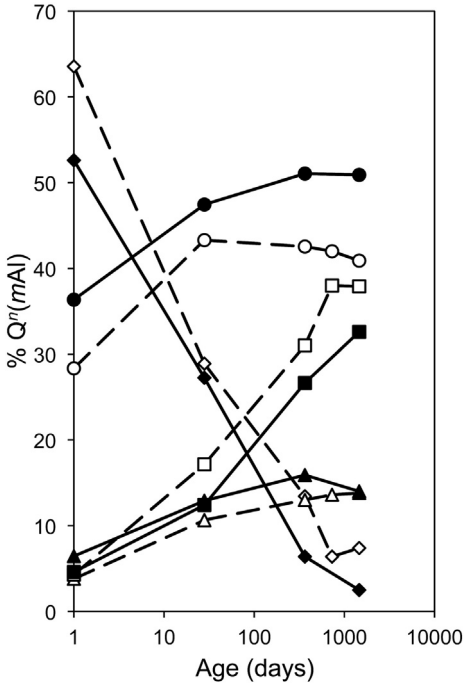

Fig. 14. The % of Si that is present as Q^0 (alite and belite; diamond), Q^1 (circle), $Q^2(1Al)$ (triangle) and $Q^2(0Al)$ (square) in neat white Portland cement pastes plotted against age for activation with water (open symbols) and KOH solution (filled symbols).

MCL, as shown in Figs. 16 and 17(a). The lengthening of MCL occurred with both methods of activation, although KOH generally resulted in slightly shorter chains for a given degree of reaction (Fig. 16), which is perhaps associated with the fact that the initial reaction with alkali activation was quicker than with water activation (Fig. 13). This increase in MCL with age (Fig. 17(a)) has been observed in many previous studies of the hydration of C_3S or Portland cement (e.g. [47,101,104–106, 108–112]). Figs. 16 and 22(a) also include points that represent the average length of just the silicate part of the chains (MCL_{Si}, calculated using Eq. (5) [47]). For comparison, Andersen et al.'s [47] data are also included on Fig. 16 (symbol ×, upper data set MCL and lower MCL_{Si}). The general trends for the data from this work are similar to those from Andersen et al. [47] although the MCL are somewhat longer at high degrees of reaction. It is notable that the values for MCL_{Si} are similar to the values for MCL of Al-free C-S-H in neat C_3S pastes e.g. [112].

Fig. 15(b) shows the normalized fraction of Si that is present in $Q^n(m\mathrm{Al})$ tetrahedra in the water-activated blend that contains 30% pfa. Comparison with Fig. 15(a) shows that the fractions of Si in Q^1, $Q^2(1Al)$ and $Q^2(0Al)$ tetrahedra were very similar in the neat and blended paste up to 28 days hydration, resulting in essentially the same MCL (Fig. 17(a)), which is not entirely consistent with the TEM-EDX data discussed in §3.3 that show clear evidence for the reaction of some of the glassy pfa by 28 days. The fraction of $Q^2(0Al)$ was very similar at all ages, the difference between the two systems after 28 days being in the fraction of Si present in end-chain tetrahedra (Q^1) or in paired tetrahedra that are adjacent to bridging tetrahedra that are occupied by Al^{3+} ions ($Q^2(1Al)$). Essentially, the fraction of $Q^2(1Al)$ in the neat cement paste remained approximately constant (about 1 in 7) throughout the period of hydration, whereas in the blend it increased rapidly from about 1 in 7 at 28 days to just over 1 in 3 at extended ages, accompanied by a decreased fraction of Q^1; the $Q^2(0Al)$ remained approximately constant after 1 year. These data indicate that the difference between the chain lengthening that occurred in the two systems was due to the incorporation of additional Al^{3+} at bridging sites in the C-A-S-H of the blend. This is evident upon inspection of the top part of Fig. 17(a), which is a plot of the site occupancy factor for the 'bridging' site (SOF_{BT}, calculated using Eq. 10 in [36]) for the water-activated neat PC (large open circle) and the blend with 30% pfa (large filled circle); the medium-sized symbols represent occupancy by Al^{3+} ($SOF_{BT}(Al)$) and the small symbols occupancy by Si^{4+} ($SOF_{BT}(Si)$).

Fig. 15(c) and (d) show the same information as Fig. 15(a) and (b) but for the alkali-activated pastes. At 1 day, the fractions of $Q^n(m\mathrm{Al})$ tetrahedra in the C-A-S-H were very similar in the neat and blended pastes, which is the same situation as occurred with water activation. However, in contrast to water activation, at 28 days the C-A-S-H in the neat cement paste and blend were not similar: whilst the fractions of $Q^2(0Al)$ were similar, the C-A-S-H in the blend contained much more $Q^2(1Al)$ and a correspondingly smaller amount of Q^1, which must be due to earlier reaction of the glassy pfa in the alkali-activated system as a consequence of the very high concentration of hydroxyl ions. The situation regarding the $Q^2(0Al)$ in the KOH-activated pastes is essentially the same as in the water activated; i.e. the fraction of $Q^2(0Al)$ was similar in the blend and the neat cement paste throughout the period of study. After 1-year hydration, the steady decrease in the fraction of Q^1 in the blend ceased and the fraction of $Q^2(1Al)$ decreased rather than continuing to increase, which was the case with water activation. This corresponds to a drop in the intensity of the peak at −71.2 ppm and so is due to the reaction of belite to produce Q^1 tetrahedra, which results in slightly shorter MCL with KOH activation than with water, which has been observed previously for C-A-S-H in KOH-activated C_3S [107] and white Portland cement [4] pastes. For the blends, the MCL was longer at 28 days with KOH activation than with water due to the incorporation of Al^{3+} ions at bridging sites in the aluminosilicate chains; the MCL is long for both at 1 year.

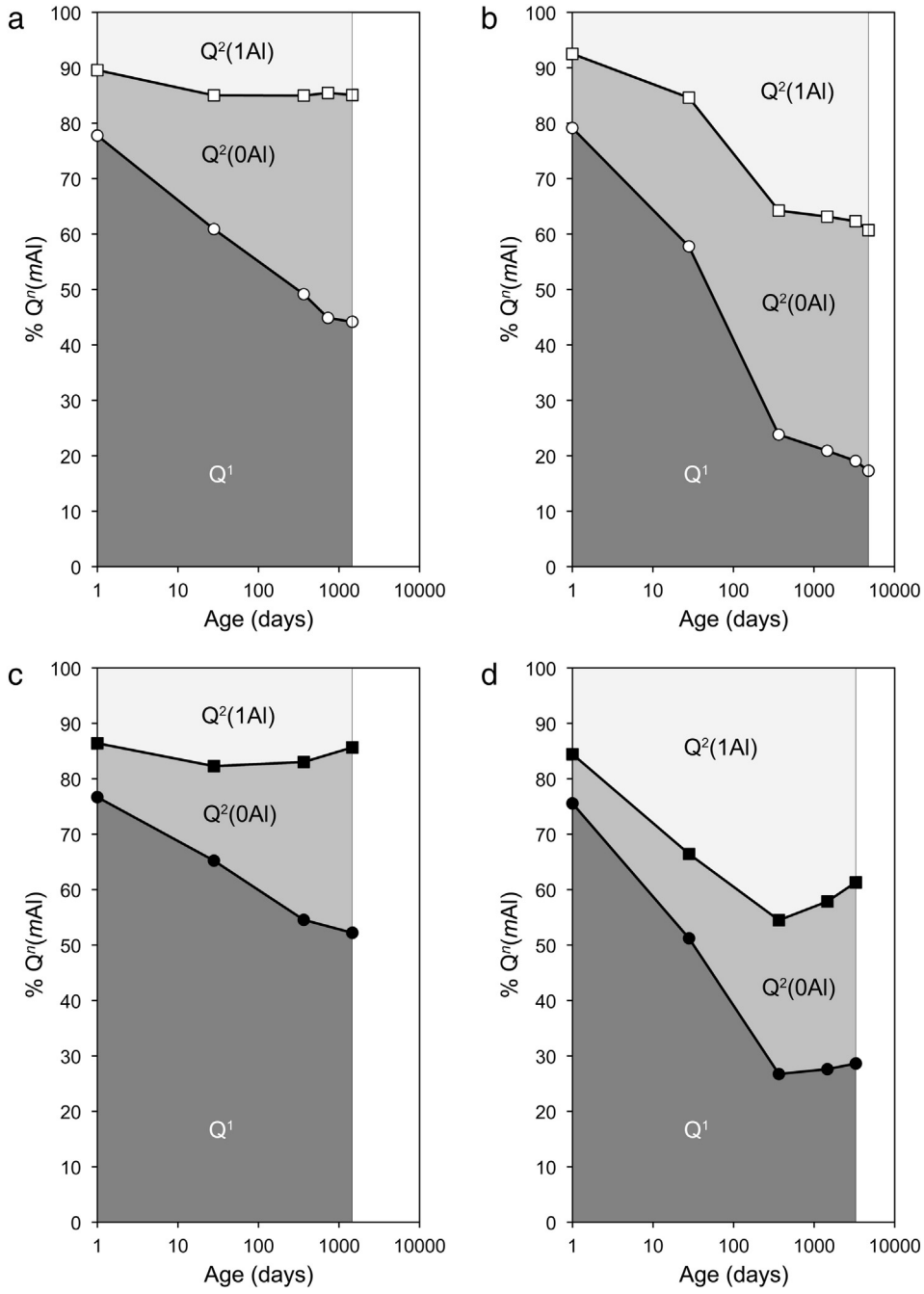

Fig. 15. The normalized fractions of Q^1 (dark shading), $Q^2(0Al)$ (medium shading) and $Q^2(1Al)$ (light shading) in the C-A-S-H at different ages for hardened pastes of (a) water-activated neat wPc, (b) water-activated 30% pfa-70% wPc, (c) KOH-activated neat wPc, and (d) KOH-activated 30% pfa-70% wPc.

The ^{29}Si NMR data for the blends are consistent with the following scheme:

At 1-day, the C-A-S-H in the water-activated blend was quite similar to that in the neat paste; the slightly higher fraction of $Q^2(1Al)$ in the alkali-activated blend is consistent with some reaction of the glassy pfa i.e. at 1 day hydration the data indicate that some pfa had reacted with alkali but not with water. Between 1 day and 1 year, the increase in the fraction of $Q^2(1Al)$ with both methods of activation is consistent with reaction of pfa in both systems. At ages greater than 1 year, the changes in the distribution of $Q^n(mAl)$ units is consistent with continued slow reaction of pfa with water activation. Whilst this may well have also occurred with alkali activation, the decrease in the fraction of $Q^2(1Al)$ was most likely due to additional dimer formed from the hydration of belite. This is reflected in a decrease in the MCL for the alkali-activated paste after 1 year (Fig. 17(b)) but a continued increase with water activation (Fig. 17(a)). It should be emphasized that these changes do not correspond to a big change in the Al/Si ratio of the C-A-S-H, which at extended ages is ≈0.2 with both methods of activation, as measured by TEM-EDX (Fig. 6). This is because although the increase in MCL might seem to be quite dramatic with water activation, in fact such increases in MCL are achieved by very modest increases in the occupation of bridging sites when the occupation of those sites is already at a high level, as shown in the top part of Fig. 17(a).

The MCL of the aluminosilicate anions in the C-A-S-H for the various cement pastes is also represented on Fig. 10, the plot of mean Al/Ca against Si/Ca ratio, where the size of the symbol is proportional to the MCL. It is evident that in general the MCL increases with age and temperature of hydration and as both the Al/Ca and Si/Ca increase.

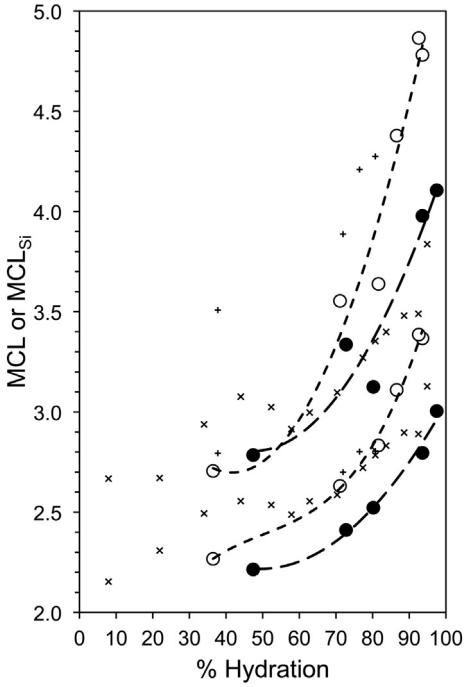

Fig. 16. Variation in MCL and MCL_{Si} with % hydration for neat white Portland cement activated by water (open circles) or KOH solution (filled circles). In both cases, the upper data are MCL and the bottom data are MCL_{Si}. The dashed lines are guides for the eye. For comparison, equivalent data are included for water-activated neat white Portland cement from [47] (×; w/c = 0.5; 20 °C) and from [106] (+; w/c = 0.425; 25 °C).

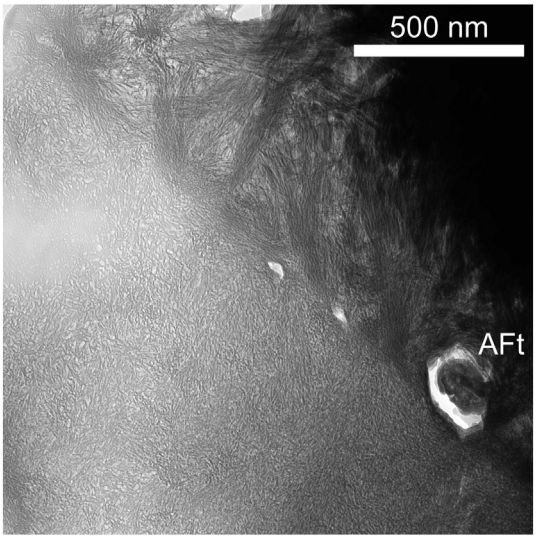

Fig. 18. TEM micrograph that shows both Ip and Op C-A-S-H in a water-activated neat wPc paste hydrated for 2 years. The interface between the two regions runs from the top left-hand corner to the bottom right. A relict of AFt is close to the bottom right hand corner; the hexagonal shape of the cross-section of the original crystal is still sharply defined, which supports the view that the surrounding C-A-S-H has been little affected by drying during specimen preparation or under the electron beam. The fine-scale morphology is typical of alite Ip C-A-S-H.

3.6. Morphology and nanostructure of C-A-S-H

It was noted in §1 that the morphology of Op C-A-S-H in ggbs/PC blends changes from fibrillar at low Si/Ca and Al/Ca ratios to foil-like at higher values, with the fineness and aspect ratio of the fibres affected by space constraints; the foil-like morphology starts to appear at a Ca/(Si + Al) ratio of about 1.2–1.3. The same composition-morphology relationship is observed in pfa/PC blends, whether reacted at elevated temperature [50] or at 25 °C (this work). Examples of fibrillar Op C-A-S-H in water-activated pastes of neat and blended cement are shown respectively in Fig. 18 (top right) and Fig. 19, which are bright field TEM images. The fibrillar morphology tends to become finer with age (it is very fine in Fig. 18), which can make it quite difficult to distinguish between Op and Ip C-A-S-H in older pastes [9].

The situation is different in alkali hydroxide-activated pastes, in which: (i) the Op C-A-S-H always has foil-like morphology (an example

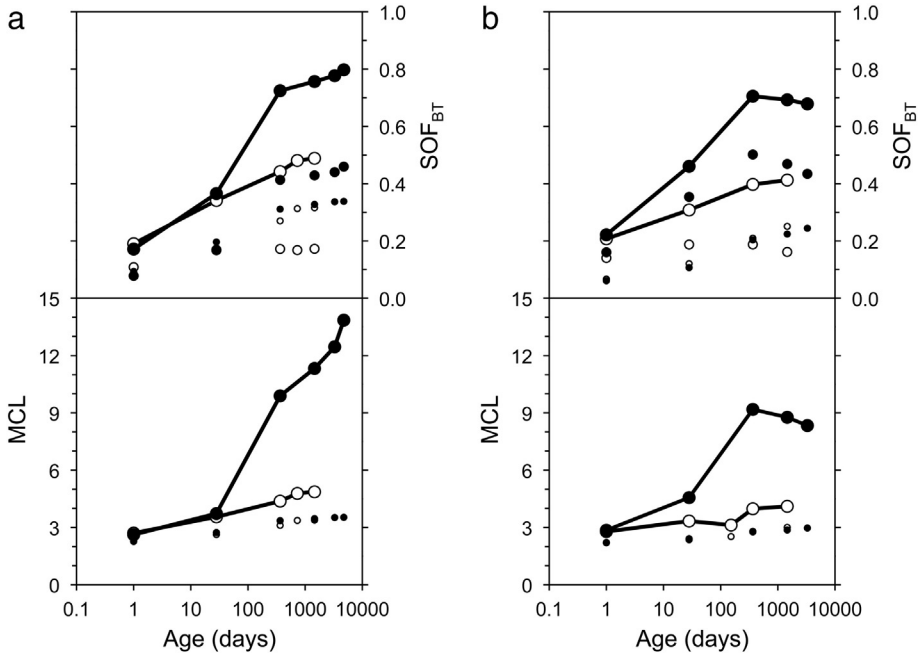

Fig. 17. (a) Variation with age of the mean aluminosilicate chain length of C-A-S-H (MCL; bottom) and the site occupancy factor for the 'bridging' site (top) in water-activated wPc (large open circle) and 70% wPc-30% pfa pastes (large filled circle). The small symbols on the MCL plot show the mean length of the silicate portions of the linear chains i.e. MCL_{Si}; the medium symbols on the SOF_{BT} plot are for SOF_{BT}(Al) and the small symbols are for SOF_{BT}(Si). (b) The same but for the KOH-activated pastes.

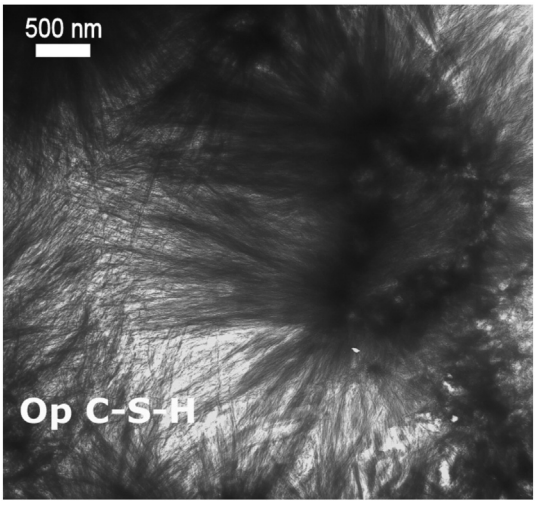

Fig. 19. TEM micrograph of Op C-S-H in the water-activated wPc-30% pfa paste reacted for 1 year. It has the fibrillar morphology that is characteristic of Op C-S-H that has Ca/(Si + Al) greater than about 1.2–1.3.

is shown in Fig. 20, right-hand side), regardless of the Ca/(Al + Si) ratio; (ii) the SAED patterns often have rings for C-S-H(I), which is related to tobermorite; and (iii) the distribution of analyses on Al/Ca-Si/Ca plots tend towards the origin. These observations are consistent with the view that higher Ca/Si ratios in alkali hydroxide-activated pastes are achieved by the interstratification of layers of CH-like structure with those of the C-A-S-H. Point (iii) is illustrated on Fig. 21 (a) and (b), which are Al/Ca-Si/Ca plots of TEM-EDX analyses of Ip (□) and Op (○) C-A-S-H present in (a) the water-activated and (b) the KOH-activated neat cement pastes hydrated for 28 days at 25 °C. The other symbols represent the compositions of tobermorite- (T) or jennite-based (J) structural units with different levels of protonation of the silicate chains: the minimum level (◇; $w/n = 0$), an intermediate level (+; $w/n = 1$), and the maximum level (×; $w/n = 2$). Points are included on the figures that represent tobermorite-based units with chain lengths of 2, 5, 8, 11, 14, 17 and ∞. Most of the units are saturated with Al (i.e. all the occupied bridging sites are occupied by Al rather than Si). The only exceptions are units with 11 tetrahedra, which in addition to those saturated with Al (i.e. Al/(Al + Si) = 3/11, which are labelled simply as T11), are also represented with one or two of the three bridging sites occupied by Al (i.e. Al/(Al + Si) = 1/11or 2/11): units with one or two Al ions are labelled as T11(1Al) and T11(2Al) respectively. T11 units with the same degree of protonation but different content of Al are joined by dotted lines. In (a) the dashed tie lines join points for T11 structural units with points on the Si/Ca axis that represent jennite-based dimer (with different degrees of protonation), and in (b) the dashed tie lines join points for structural units of the same length but different degrees of protonation with CH (i.e. at the origin); in fact, for this particular paste, the tie line is most likely between CH and a mixture of T2 and T5 since from NMR the mean length of the aluminosilicate anions is only 3.4.

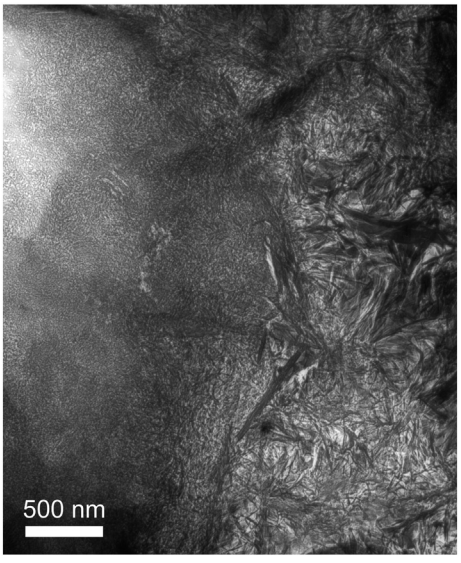

Fig. 20. TEM micrograph of Ip C-S-H (left) and Op C-S-H (right) in the alkali-activated wPc-30% pfa paste reacted for 4 years. The Op C-S-H has the foil-like morphology that is characteristic of C-S-H(I). The Ip C-S-H has the fine-scale morphology that is typical of alite Ip C–S–H.

Since TEM-EDX data for C-A-S-H in water-activated pastes – such as those shown in Fig. 21(a) – are consistent with the T/J nanostructural approach, it is tempting to associate foil-like Op morphology in water-activated pastes with tobermorite-based structure and fibrillar Op morphology with jennite-based [58]. However, it is important to note that other morphologies also occur in these systems. Bright-field imaging in the TEM has shown that Ip C-A-S-H that is formed from the reaction of larger alite grains typically has a rather homogenous fine-scale morphology; whether in pastes of neat Portland cement [3], ggbs/PC blends [7], or in pfa/PC blends reacted at 55 °C [98]. Unsurprisingly, this morphology was also observed in the pfa/PC blends studied in this work, hydrated at 25 °C, whether activated with water (e.g. see Fig. 18 for neat cement and Fig. 22 for a blend) or alkali hydroxide (e.g. see Fig. 20, left-hand side). Ip C-A-S-H that is present in small, fully reacted particles typically has foil-like morphology (e.g. see [50, 113]), although it often has a linear, spoke-wheel appearance when formed from pfa particles, whether activated using water or alkali hydroxide, which is illustrated in Fig. 9 (large micrograph for KOH activation and inset micrograph for water activation). The partially reacted pfa particle shown in Fig. 7 is a good example of Ip C-A-S-H that has mixed morphology: foil-like in the centre and fibrillar around the edges, the latter being consistent with examples of less well-reacted particles observed by other workers [114–116]. As noted above, such a mixture of fibrillar and foil-like morphologies is also a commonly observed characteristic of Op C-A-S-H in water-activated pastes when the mean Ca/(Si + Al) ratio is less than about 1.2–1.3. The main exception to this observation is the Op C-A-S-H that is formed in neat ggbs pastes, which is entirely foil-like. This is evident from inspection of Fig. 23(a), which is a plot of mean Ca/(Si + Al) ratio (Op and Ip) against the reciprocal MCL for the C-A-S-H that is present in blends that contain pfa (circles), metakaolin (diamond), or ggbs (triangles); open symbol = entirely fibrillar morphology; half-filled symbol = mixed fibrillar/foil-like morphology; filled symbol = entirely foil-like morphology. The lines on the figure represent the possible combinations of composition and aluminosilicate chain length for jennite-based (the quadrilateral C–E–W–U) and tobermorite-based (F–H–Z–X (or –X′)) nanostructural models; see [16,17,58] for a detailed explanation of the figure and the nanostructural models, which have recently been used to help improve the structural consistency of thermodynamic models for C-(A-)S-H [117,118]. It is evident that points for mixed morphology occur in the region for purely tobermorite-based structure, which as a consequence cannot be associated with Op C-A-S-H that has exclusively foil-like morphology and an alternative explanation must be sought for the transition to foils that occurs as the Ca/(Si + Al) ratio drops. The equivalent plot for the KOH-activated pastes is shown in Fig. 23(b); the symbols are all filled because the Op C-A-S-H in such systems is always foil-like, regardless of composition, although it is also evident that there are no points in the region for exclusively jennite-based structure. A number of the points fall essentially along the line H–Z, which corresponds to tobermorite-based structural units that are totally protonated, although it is plausible that some of the charge compensation is provided by K^+ ions.

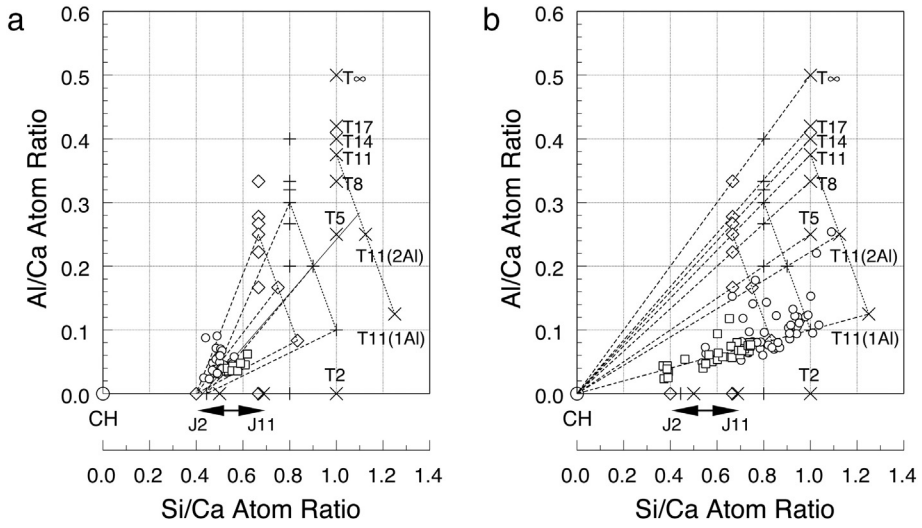

Fig. 21. Al/Ca against Si/Ca atom ratio plots of TEM-EDX analyses of Ip (□) and Op (○) C-A-S-H present in (a) the water-activated and (b) the KOH-activated neat cement pastes hydrated for 28 days at 25 °C.

The Ca/(Si + Al) ratios from Fig. 23(a) are replotted in Fig. 24 against the %CH present in the pastes. Whilst there is some scatter in the data – which is to be expected given the range of cement compositions involved – it is nevertheless clear that in general the Ca/(Si + Al) ratio decreases with decreasing %CH; from ≈1.75 when the CH content is high (≈30%) to ≈0.9 when there is no CH. It is evident from the positions of the symbols that are half-filled that the transition from purely fibrillar Op morphology to a mixture of fibrillar and foil-like morphology occurs when the quantity of CH in a paste is between 8 and 13%, if the percentage is expressed on the basis of ignited weight and when calculated using the 'tangent' analysis method that accounts for the mass loss associated with the concurrent dehydration of other phases [51–53].

Rodriguez et al. [119] attempted recently to establish the relationship between the chemical composition, silicate anion structure and morphology of C-S-H by studying preparations that had been synthesized either via silica-lime reactions or by the hydration of C_3S under controlled lime concentrations. In their synthesis procedures, Rodriguez et al. [119] used filtered lime solutions for concentrations up to 20 mmol L^{-1} and used filtered solutions obtained from suspensions of hydrating C_3S for concentrations of 22, 25 and 27 mmol L^{-1}. This is because the solubility of CH is about 20 mmol L^{-1}, although it varies somewhat with temperature, decreasing linearly with increasing temperature: regression analysis of data from [120] gives Eq. (9), where the solubility, *S*, is in mmol L^{-1} CaO and temperature, *T*, is in °C.

$$S = 23.65573 - 0.14507(T) \quad (r^2 = 0.998) \tag{9}$$

The solubility of CH at 25 °C calculated using Eq. (9) is 20.03 mmol L^{-1}. The values from [120] that were used for Eq. (9) were measured using large crystals – and are consistent with measurements by other workers (e.g. [121,122]) – but higher apparent solubilities were observed when very fine crystals were used, up to at least 25 and 22 mmol L^{-1} at 5 °C and 25 °C respectively [120]. Duchesne & Reardon [123] presumed this to be due to a high surface energy of CH crystals in water, with the surface energy of fine particles contributing to an overall increase in the Gibbs free energy of formation and thus to an enhancement in its solubility. As a consequence, the apparent solubility of CH in hardened cement pastes is likely to be enhanced when the crystals are very small. Rodriguez et al. [119] found that all of their samples prepared via silica-lime reactions with bulk Ca/Si up to 1.5 had foil-like morphology; a sample with Ca/Si ≈1.58 prepared at [CaO] = 22 mmol L^{-1} had mixed fibrillar/foil morphology; and samples with Ca/Si ≈1.61 and ≈1.63 prepared respectively at [CaO] = 25 and 27 mmol L^{-1} had entirely fibrillar morphology. Since Rodriguez et al. [119] observed a link between morphology and the concentration of CaO in solution, it is instructive to compare the values for [CaO] used in their procedures with those present in the pore solutions of hardened cement pastes, which can be extracted using a high pressure device, first used by Longuet et al. [124]. Whilst there has been some debate about the validity of the technique (e.g. [125–129]), it is the only practical method for accessing the aqueous phase of hardened cements and has therefore been adopted widely [e.g. 81,92,94,124–150]. In water-activated neat Portland cement pastes, whilst the concentration of Ca in extracted pore solutions has been observed to reduce from >20 mmol L^{-1} at early age to <2 mmol L^{-1} at extended ages (because of the release of alkalis [92,145,149,151,152]), the solutions nevertheless remain oversaturated with respect to CH to extended times [92,145,151,153]. It is relevant that TEM studies have consistently shown the Op C-A-S-H in such systems to have fibrillar morphology [3,4,9,14,48,58,154] and C-S-H with fibrillar morphology has also been observed by transmission soft X-ray microscopy to form when particles of C_3S or

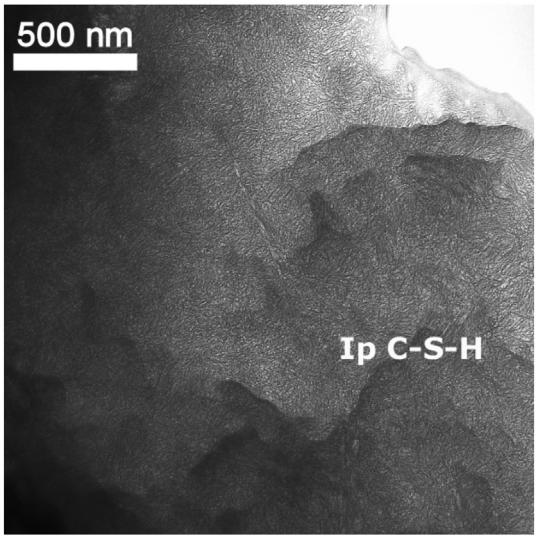

Fig. 22. TEM micrograph of a region in the 1-month-old wPc-30% pfa paste that shows the fine-scale morphology that is typical of alite Ip C–S–H.

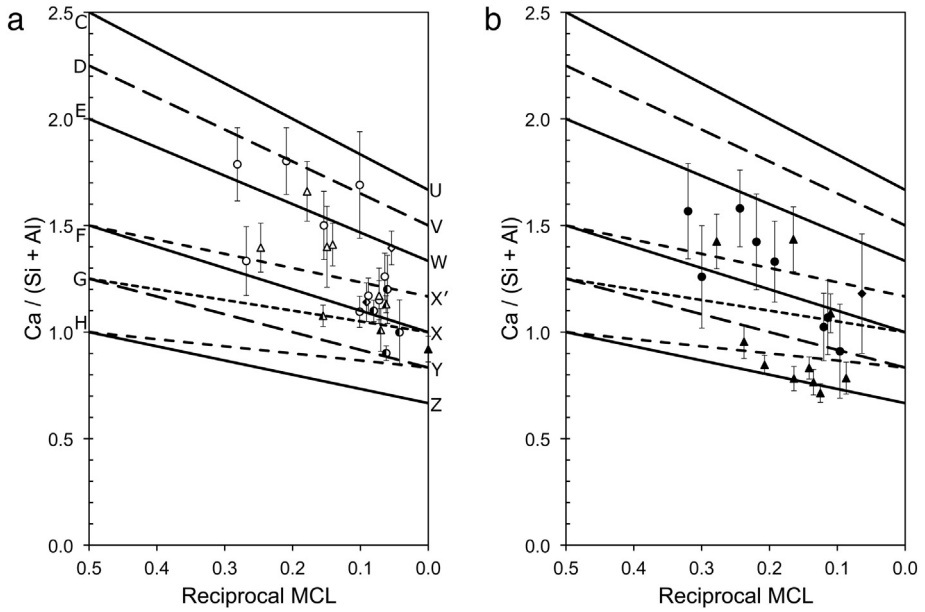

Fig. 23. Plots of mean Ca/(Si + Al) ratio (Op and Ip) against the reciprocal MCL for the C-A-S-H that is present in (a) water-activated and (b) KOH-activated blends that contain pfa (circles), metakaolin (diamond), or ggbs (triangles) (open symbol = entirely fibrillar morphology; half-filled symbol = mixed fibrillar/foil-like morphology; filled symbol = entirely foil-like). The data are from this work and [6,8,49,50,56,97,98].

silica react in solutions saturated or supersaturated with respect to CH [155–157] (the morphology sometimes described as 'sheaf-of-wheat').

Pore solutions have also been extracted from hardened cement pastes that contain pfa [92,126,128,138–141,144,148]. In particular, Deschner et al. [92] expressed pore solutions from 50% oPc-50% pfa pastes and calculated 'effective' saturation indices (defined in [129]) for various hydration products. Whilst the solutions from early-age samples were slightly oversaturated with respect to CH, the saturation index started to decrease after 7 days hydration and became undersaturated between 28 and 90 days, which they associated with the consumption of CH by the pozzolanic reaction, in agreement with Goñi et al. [139]. This association is illustrated on Fig. 25(a), which is a plot of $CH^{act.}/CH^{exp.}$ against the 'effective' saturation index for CH using data from [81,92] for the peak and subsequent values of $CH^{act.}/CH^{exp.}$ An 'effective' saturation index of 0 indicates that there is equilibrium between the solid and liquid, a positive value indicates that the solution is oversaturated, and a negative value indicates that it is undersaturated [129]. It is evident that the 'effective' saturation index for CH started to fall after the peak value in CH^{act}/CH^{exp} had been reached and turned negative – i.e. the solution became undersaturated with respect to CH – when the value of CH^{act}/CH^{exp} subsequently dropped below 0.85, which coincided with the concentration of Si in solution increasing above 0.35 mmol L^{-1}, Fig. 25(b). Since the TEM results from the present study indicate that in such systems the Op C-A-S-H would have mixed fibrillar/foil-like morphology, this indicates that the appearance of foil-like morphology in water-activated pastes is associated with a pore solution that is undersaturated with respect to CH – in agreement with the results of Rodriguez et al. [119] for synthetic C-S-H – and that has a concentration of Si in solution above about 0.35 mmol L^{-1} and Ca/(Si + Al) ratio in solution that is less than about 2.5 [81,92], which is about twice the value for the C-A-S-H. This appearance of foil-like morphology and the decrease in the %CH below 8–13% also coincides with a reduction in the pH of the extracted pore solution, as shown in Fig. 26 (data from [81,92,94]), which is a plot of the pH of pore solutions extracted from water-activated oPc and pfa-oPc pastes against %CH; crosses are placed over the data for the pfa-oPc pastes that are older than 7 days, thus representing pastes where the glassy pfa had probably started to react. Pore-solution extraction is of course a bulk technique, which at best gives an average composition for the pore solution that is present in a paste [125,126]. It is therefore possible that in addition to the changes in the average pore-solution composition that occur with age, the solution composition might vary with microstructural location, which could plausibly also contribute to the development of mixed C-A-S-H morphologies [119], as well as the effect that space constraints have upon growth [3,7]. This would seem to be supported by the results of a ^{29}Si MAS NMR study of a mixture of C_3S and silica in which the reactants were selectively enriched with ^{29}Si [158]. It was found that the Si atoms from the two components were not equilibrated throughout the hydration products but rather

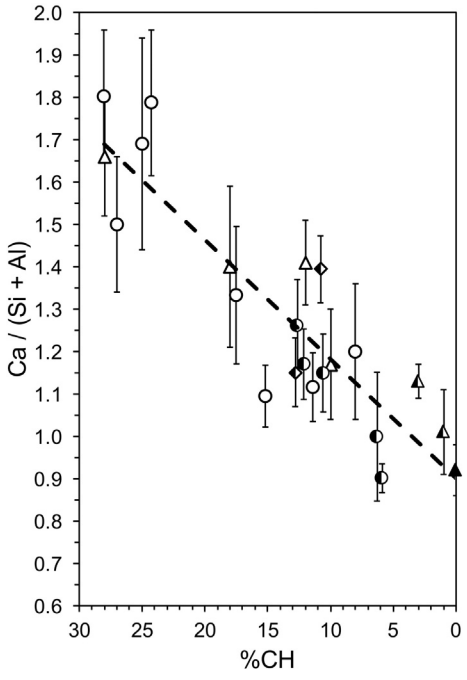

Fig. 24. Plot of the Ca/(Si + Al) ratios from Fig. 23(a) against the %CH. The CH axis is reversed to facilitate comparison with Fig. 23. The dashed line is a guide for the eye.

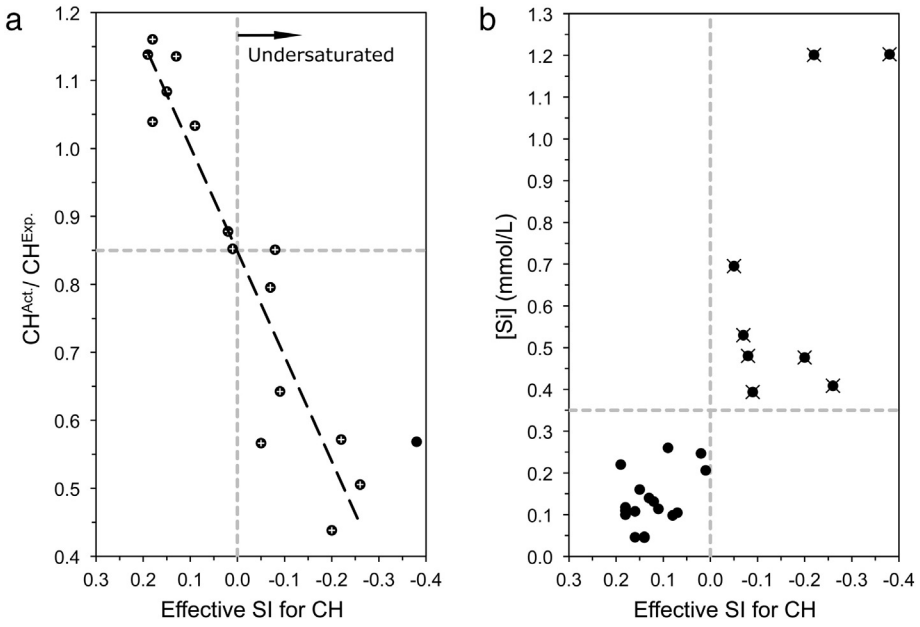

Fig. 25. (a) Plot of $CH^{act.}/CH^{exp.}$ against the effective saturation index for calcium hydroxide. The data are from [81,92] and only include those for the peak and subsequent values of $CH^{act.}/CH^{exp.}$ An effective saturation index of 0 indicates that there is equilibrium between the solid and liquid, a positive value indicates that the solution is oversaturated and a negative value indicates that it is undersaturated [129]. The dashed line is the result of the linear regression analysis of all but one of the data points (i.e. the data indicated with white +). The horizontal axis is reversed to facilitate comparison with Figs. 23 and 24. (b) Plot of [Si] against the effective saturation index for calcium hydroxide for the pore solutions expressed from hardened pastes of water-activated pfa-oPc blends (filled circles). Crosses are placed over the data for the pfa-oPc pastes that have values of $CH^{act.}/CH^{exp.} < 0.85$. The data are from [81,92].

were preferentially located in distinct species. In particular, it was concluded that the part of the C-S-H that formed from the silica had longer MCL and a slightly better ordered structure than the remainder.

It would appear that Op C-A-S-H with foil-like morphology forms in water-activated pfa-oPc pastes when the glassy pfa has reacted to such an extent that the quantity of CH has decreased significantly and the average composition of the pore solution has changed, with a drop in pH, undersaturation with respect to CH, and much higher concentration of Si (above about 0.35 mmol L^{-1}). It seems plausible that the change in composition of the pore solution results in a transition from essentially one-dimensional growth of the C-S-H particles to two-dimensional; i.e., long thin particles (aggregations of which form fibrils) to foils [58].

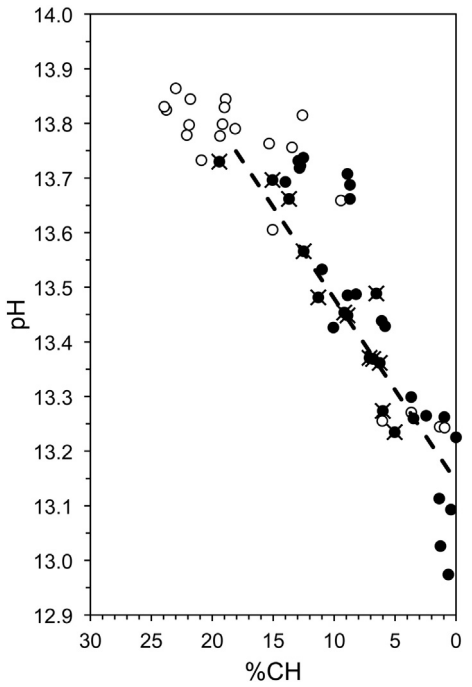

Fig. 26. Plot of pH of the extracted pore solution against %CH for pfa-PC blends (filled circles) and the associated neat PC pastes (open circles). Crosses are placed over the data for the pfa-PC pastes that are older than 7 days, and thus represent pastes where the glassy pfa has started to react. The data are from [81,92,94].

4. Summary and conclusions

This article reports the results of a multi-technique study focussed on the evolution of the two main hydration products in water- and alkali-activated white Portland cement pastes (wPc) and blends of wPc with low-calcium pulverized fuel ash (pfa) reacted at 20–25 °C for up to 13 years. In summary:

(i) The main products in the wPc and 70% wPc-30% pfa pastes were C-S-H, CH and ettringite for hydration with water, and C-A-S-H and microcrystalline CH for hydration with KOH solution. AFm-type phases were not detected by XRD in any of the systems but a peak assigned to $Al^{[6]}$ in AFm is present on all ^{27}Al NMR spectra indicating that there was either too little AFm in the pastes or the crystals were not sufficiently large or ordered to be detected by XRD. Peaks are also present on the ^{27}Al NMR spectra for both methods of activation that are assigned to the 'third aluminate hydrate'.

(ii) The reaction of wPc with water was initially retarded in the presence of pfa particles but accelerated at intermediate ages, the latter being consistent with the so-called 'filler effect'. Reaction with KOH solution was rapid with or without pfa.

(iii) The quantity of CH in wPc-pfa pastes was still reducing at 13 years hydration, indicating that glassy pfa continues to react over extended ages.

(iv) The chemical composition of C-A-S-H was measured free of intermixture with other phases using TEM-EDX. For reaction with water, the mean Ca/Si at extended ages was ≈1.9 for neat wPc and ≈1.35 for the 70% wPc-30% pfa blend; the values were lower with KOH solution. The mean Al/Si at extended ages was ≈0.05 for neat wPc and ≈0.20 for the 70% wPc-30% pfa blend; the values were similar with water or KOH solution. A significant amount of glassy pfa had reacted by 28 days.

(v) A linear relationship was observed between the Si/Ca and Al/Ca ratios of the C-A-S-H (Eq. (6)) that is very similar to the one determined previously for blends with ggbs, suggesting strongly that there is a universal compositional relationship for the C-A-S-H in blends of Pc with aluminosilicate-rich supplementary cementitious materials.

(vi) Excellent agreement was found between the Al/Si of C-A-S-H calculated from the results of the deconvolution of ^{29}Si NMR spectra and values measured directly by TEM-EDX, which supports the assignment of the peak at ≈ -82 ppm entirely to $Q^2(1Al)$ for these systems.

(vii) The fractions of $Q^n(m\text{Al})$ units in the C-A-S-H in the wPc and 70% wPc-30% pfa pastes varied with age as follows: Q^1 was dominant and similar at early age, decreased in both with age, but the decrease was greater in the blend; $Q^2(0Al)$ was similar at all ages; $Q^2(1Al)$ was about 1 in 7 in both at early age, remained the same in the wPc with age but increased in the blend to >1 in 3 at extended age. The principal difference in chain lengthening between the two was the incorporation of additional Al^{3+} at bridging sites in the blend. The MCL lengthened with age, as both the Al/Ca and Si/Ca increased, and – from previous studies – with the temperature of hydration.

(viii) Bright-field imaging in the TEM showed that the morphology of outer product C-A-S-H was always foil-like with KOH solution, regardless of chemical composition, and the distribution of EDX analyses on Al/Ca-Si/Ca plots is consistent with T/CH nanostructural models. With water, outer product C-A-S-H had fibrillar morphology at high Ca/(Si + Al) ratios and foil-like morphology started to appear in the blend when Ca/(Si + Al) $\approx$1.2–1.3 and %CH $\approx$8–13; the Ca/(Si + Al) decreased from $\approx$1.75 at 30% CH to $\approx$0.9 when there was no CH. Comparison with literature data indicates that the appearance of foil-like morphology is associated with a pore solution that is reducing in pH, undersaturated with respect to CH and that has a concentration of Si that is > $\approx$0.35 mmol L^{-1}. Foil-like morphology cannot be associated with entirely T-based structure.

Acknowledgements

Thanks are due to the Nuclear Decommissioning Authority for financial support; to the Engineering and Physical Sciences Research Council for funding under Grant Nos. GR/S45874/01 and GR/R07073/01 and for a studentship (RT); to Dr. M. Zhang-Williams, Dr. C.A. Love, Dr. H.M. Dyson and Mr. J. Boomer for some of the experimental work; to a number of industrial collaborators for additional financial and technical support (Castle Cement, Lafarge, and W.R. Grace); and to Dr. D.C. Apperley at Durham University's EPSRC-funded NMR service for collection of the ^{27}Al NMR spectra.

References

[1] H.F.W. Taylor, The Chemistry of Cements, 1Academic Press, London, 1964.
[2] J.F. Young, W. Hansen, Volume relationships for C–S–H formation based on hydration stoichiometries, Mater. Res. Soc. Symp. Proc. 85 (1987) 313–322.
[3] I.G. Richardson, G.W. Groves, The microstructure and microanalysis of hardened ordinary Portland cement pastes, J. Mater. Sci. 28 (1993) 265–277.
[4] I.G. Richardson, The nature of the hydration products in hardened cement pastes, Cem. Concr. Comp. 22 (2000) 97–113.
[5] H.F.W. Taylor, Cement Chemistry, second ed. Thomas Telford, London, 1997.
[6] I.G. Richardson, G.W. Groves, The structure of the calcium silicate hydrate phases present in hardened pastes of white Portland cement/blast-furnace slag blends, J. Mater. Sci. 32 (1997) 4793–4802.
[7] I.G. Richardson, G.W. Groves, The microstructure and microanalysis of hardened cement pastes involving ground granulated blast-furnace slag, J. Mater. Sci. 27 (1992) 6204–6212.
[8] I.G. Richardson, The structure of C–S–H in hardened slag cement pastes, Proc. 10th Int. Cong. Chem. Cem., 2, Göteborg 1997, p. 2ii068 (8pp).
[9] R. Taylor, I.G. Richardson, R.M.D. Brydson, Composition and microstructure of 20-year-old ordinary Portland cement-ground granulated blast-furnace slag blends containing 0 to 100% slag, Cem. Concr. Res. 40 (2010) 971–983.
[10] I.G. Richardson, S.A. Rodger, G.W. Groves, The microstructure of ggbfs/OPC hardened cement pastes and some effects of leaching, Mater. Res. Soc. Symp. Proc. 176 (1990) 63–74.
[11] L.S. Dent-Glasser, E.E. Lachowski, M.Y. Qureshi, H.P. Calhoun, D.J. Embree, W.D. Jamieson, C.R. Masson, Identification of some of the polysilicate components of trimethylsilylated cement paste, Cem. Concr. Res. 11 (1981) 775–780.
[12] K. Mohan, H.F.W. Taylor, A trimethylsilylation study of tricalcium silicate pastes, Cem. Concr. Res. 12 (1982) 25–31.
[13] J. Hirljac, Z.-Q. Wu, J.F. Young, Silicate polymerization during the hydration of alite, Cem. Concr. Res. 13 (1983) 877–886.
[14] I.G. Richardson, The nature of C–S–H in hardened cements, Cem. Concr. Res. 29 (1999) 1131–1147.
[15] H.F.W. Taylor, Proposed structure for calcium silicate hydrate gel, J. Am. Ceram. Soc. 69 (1986) 464–467.
[16] I.G. Richardson, G.W. Groves, Models for the composition and structure of calcium silicate hydrate (C–S–H) gel in hardened tricalcium silicate pastes, Cem. Concr. Res. 22 (1992) 1001–1010.
[17] I.G. Richardson, G.W. Groves, The incorporation of minor and trace elements into calcium silicate hydrate (C–S–H) gel in hardened cement pastes, Cem. Concr. Res. 23 (1993) 131–138.
[18] I.G. Richardson, A.R. Brough, R.M.D. Brydson, G.W. Groves, C.M. Dobson, The location of aluminium in substituted calcium silicate hydrate (C–S–H) gels as determined by ^{29}Si and ^{27}Al NMR and EELS, J. Am. Ceram. Soc. 76 (1993) 2285–2288.
[19] M.D. Andersen, H.J. Jakobsen, J. Skibsted, Incorporation of aluminum in the calcium silicate hydrate (C-S-H) of hydrated Portland cements: A high-field Al-27 and Si-29 MAS NMR Investigation, Inorg. Chem. 42 (2003) 2280–2287.
[20] G.K. Sun, J.F. Young, R.J. Kirkpatrick, The role of Al in C-S-H: NMR, XRD, and compositional results for precipitated samples, Cem. Concr. Res. 36 (2006) 18–29.
[21] F. Liebau, Structural Chemistry of Silicates – Structure, Bonding, and Classification, Springer-Verlag, Berlin, 1985.
[22] E. Bonaccorsi, S. Merlino, A.R. Kampf, The crystal structure of tobermorite 14 Å (plombierite), a C–S–H phase, J. Am. Ceram. Soc. 88 (2005) 505–512.
[23] S. Merlino, E. Bonaccorsi, T. Armbruster, The real structures of clinotobermorite and tobermorite 9 Å: OD character, polytypes, and structural relationships, Eur. J. Mineral. 12 (2000) 411–429.
[24] M.J. Buerger, The determination of the crystal structure of pectolite, $Ca_2NaHSi_3O_9$, Z. Krist. 108 (1956) 248–262.
[25] M.J. Buerger, C.T. Prewitt, The crystal structure of wollastonite and pectolite, Proc. Natl. Acad. Sci. 47 (1961) 1884–1888.
[26] M.J. Buerger, C.T. Prewitt, Comparison of the crystal structures of wollastonite and pectolite, Mineral. Soc. Amer. Spec. Paper 1, 3rd General Meeting Int. Mineral. Ass. 1963, pp. 293–302.
[27] C.T. Prewitt, Refinement of the structure of pectolite, $Ca_2NaHSi_3O_9$, Z. Krist. 125 (1967) 298–316.
[28] W.F. Müller, On stacking disorder and polytypism in pectolite and serandite, Z. Krist. 144 (1976) 401–408.
[29] Y. Takeuchi, Y. Kudoh, Hydrogen bonding and cation ordering in Magnet Cove pectolite, Z. Krist. Krist. Krist. Krist. 146 (1977) 281–292.
[30] Y. Ohashi, L.W. Finger, The role of octahedral cations in pyroxenoid crystal chemistry. I. Bustamite, wollastonite, and the pectolite-schizolite-serandite series, Am. Mineral. 63 (1978) 274–288.
[31] Y. Ohashi, Polysynthetically-twinned structures of enstatite and wollastonite, Phys. Chem. Miner. 10 (1984) 217–229.
[32] F.J. Trojer, The crystal structure of parawollastonite, Z. Krist. 127 (1968) 291–308.
[33] Y.-S. Dai, J.E. Post, Crystal structure of hillebrandite: a natural analogue of calcium silicate hydrate (CSH) phases in Portland cement, Am. Mineral. 80 (1995) 841–844.
[34] J.A. Gard, H.F.W. Taylor, The crystal structure of foshagite, Acta Cryst. 13 (1960) 785–793.
[35] E. Bonaccorsi, S. Merlino, H.F.W. Taylor, The crystal structure of jennite, $Ca_9Si_6O_{18}(OH)_6 \cdot 8H_2O$, Cem. Concr. Res. 34 (2004) 1481–1488.
[36] I.G. Richardson, Model structures for C–(A)–S–H(I), Acta Crystallogr. B70 (2014) 903–923.
[37] H. Stade, On the structure of ill-crystallized calcium hydrogen silicates.II. A phase consisting of poly- and disilicate, Z. Anorg. Allg. Chem. 470 (1980) 69–83 (in German).
[38] H. Stade, W. Wieker, On the structure of ill-crystallized calcium hydrogen silicates. I. Formation and properties of an ill-crystallized calcium hydrogen disilicate phase, Z. Anorg. Allg. Chem. 466 (1980) 55–70 (in German).
[39] H. Stade, W. Wieker, G. Garzo, On the structure of ill-crystallized calcium hydrogen silicates. IV. Anion composition of the hydration products of tricalcium silicate, Z. Anorg. Allg. Chem. 500 (1983) 123–131.
[40] H. Stade, D. Müller, G. Scheler, On the structure of ill-crystallized calcium hydrogen silicates. V. Studies on the coordination of Al in CSH(di,poly) by 27Al NMR spectroscopy, Z. Anorg. Allg. Chem. 510 (1984) 16–24.
[41] H. Stade, A.-R. Grimmer, G. Engelhardt, M. Magi, E. Lippmaa, On the structure of ill-crystallized calcium hydrogen silicates. VII. Solid state silicon-29 NMR studies on C-S-H (Di,Poly), Z. Anorg. Allg. Chem. 528 (1985) 147–151 (in German).
[42] H. Stade, D. Müller, On the coordination of Al in ill-crystallized C-SH phases formed by hydration of tricalcium silicate and by precipitation reactions at ambient temperature, Cem. Concr. Res. 17 (1987) 553–561.

[43] X. Cong, R.J. Kirkpatrick, ^{1}H-^{29}Si CPMAS NMR study of the structure of calcium silicate hydrate, Adv. Cem. Res. 7 (1995) 103–111.
[44] F. Brunet, Ph. Bertani, Th. Charpentier, A. Nonat, J. Virlet, Application of ^{29}Si homonuclear and ^{1}H-^{29}Si heteronuclear NMR correlation to structural studies of calcium silicate hydrates, J. Phys. Chem. B 108 (2004) 15494–15502.
[45] I.G. Richardson, A.R. Brough, G.W. Groves, C.M. Dobson, The characterization of hardened alkali-activated blast-furnace slag pastes and the nature of the calcium silicate hydrate (C–S–H) phase, Cem. Concr. Res. 24 (1994) 813–829.
[46] G. Engelhardt, D. Michel, High Resolution Solid-State NMR of Silicates and Zeolites, Wiley, New York, 1987.
[47] M.D. Andersen, H.J. Jakobsen, J. Skibsted, Characterization of white Portland cement hydration and the C-S-H structure in the presence of sodium aluminate by ^{27}Al and ^{29}Si MAS NMR spectroscopy, Cem. Concr. Res. 34 (2004) 857–868.
[48] R. Taylor, I.G. Richardson, R.M.D. Brydson, Nature of C-S-H in 20 year old neat ordinary Portland cement and 10% Portland cement—90% ground granulated blast furnace slag pastes, Adv. Appl. Ceram. 106 (2007) 294–301.
[49] A.V. Girão, I.G. Richardson, C.B. Porteneuve, R.M.D. Brydson, Morphology and nanostructure C–S–H in white Portland cement-fly ash hydrated at 85 °C, Adv. Appl. Ceram. 106 (2007) 283–293.
[50] A.V. Girão, I.G. Richardson, R. Taylor, R.M.D. Brydson, Composition, morphology and nanostructure of C–S–H in 70% white Portland cement-30% fly ash blends hydrated at 55 °C, Cem. Concr. Res. 40 (2010) 1350–1359.
[51] P.J. Le Sueur, Studies of the hydration of tricalcium silicatePhD thesis University of Oxford, UK, 1984.
[52] B.K. Marsh, Relationships between engineering properties and microstructural characteristics of hardened cement paste containing pulverized-fuel ash as a partial cement replacementPhD thesis Hatfield Polytechnic, UK, 1984.
[53] B.K. Marsh, R.L. Day, Pozzolanic and cementitious reactions of fly ash blended cement pastes, Cem. Concr. Res. 18 (1988) 301–310.
[54] J.A. Forrester, A conduction calorimeter for the study of cement hydration, Soc. Chem. Ind. Meeting, December 16th 1965.
[55] J.A. Forrester, A conduction calorimeter for the study of cement hydration, Cem. Technol. 1 (1970) 95–99.
[56] C.A. Love, I.G. Richardson, A.R. Brough, Composition and structure of C-S-H in white Portland cement-20% metakaolin pastes hydrated at 25 °C, Cem. Concr. Res. 37 (2007) 109–117.
[57] J. Chudek, G. Hunter, M. Jones, S. Scrimgeour, P. Hewlett, A. Kudryavtsev, Aluminium-27 solid state NMR spectroscopic studies of chloride binding in Portland cement and blends, J. Mater. Sci. 35 (2000) 4275–4288.
[58] I.G. Richardson, Tobermorite/jennite- and tobermorite/calcium hydroxide-based models for the structure of C–S–H: applicability to hardened pastes of tricalcium silicate, beta-dicalcium silicate, Portland cement, and blends of Portland cement with blast-fumace slag, metakaolin, or silica fume, Cem. Concr. Res. 34 (2004) 1733–1777.
[59] P.W. Brown, J.V. Bothe, The stability of ettringite, Adv. Cem. Res. 5 (1993) 47–63.
[60] J. Skibsted, E. Henderson, H.J. Jakobsen, Characterization of calcium aluminate phases in cements by aluminum-27 MAS NMR spectroscopy, Inorg. Chem. 32 (1993) 1013–1027.
[61] M.D. Andersen, H.J. Jakobsen, J. Skibsted, A new aluminium-hydrate species in hydrated Portland cements characterized by ^{27}Al and ^{29}Si MAS NMR spectroscopy, Cem. Concr. Res. 36 (2006) 3–17.
[62] Z. Dai, T.T. Tran, J. Skibsted, Aluminum incorporation in the C–S–H phase of white Portland cement-metakaolin blends studied by ^{27}Al and ^{29}Si MAS NMR Spectroscopy, J. Am. Ceram. Soc. 97 (2014) 2662–2671.
[63] B. Lothenbach, K.L. Scrivener, R.D. Hooton, Supplementary cementitious materials, Cem. Concr. Res. 41 (2011) 1244–1256.
[64] E. Berodier, K. Scrivener, Understanding the filler effect on the nucleation and growth of C-S-H, J. Am. Ceram. Soc. 97 (2014) 3764–3773.
[65] S.S. Beedle, G.W. Groves, S.A. Rodger, The effect of fine pozzolanic and other particles on the hydration of C_3S, Adv. Cem. Res. 2 (1989) 3–8.
[66] W.A. Gutteridge, J.A. Dalziel, Filler cement: the effect of the secondary component on the hydration of Portland cement. Part I: A fine non-hydraulic filler, Cem. Concr. Res. 20 (1990) 778–782.
[67] W.A. Gutteridge, J.A. Dalziel, Filler cement: the effect of the secondary component on the hydration of Portland cement. Part 2: Fine hydraulic binders, Cem. Concr. Res. 20 (1990) 853–861.
[68] H. Moosberg-Bustnes, B. Lagerblad, E. Forssberg, The function of fillers in concrete, Mater. Struct. 37 (2004) 74–81.
[69] D.P. Bentz, Modeling the influence of limestone filler on cement hydration using CEMHYD3D, Cem. Concr. Compos. 28 (2006) 124–129.
[70] T. Oey, A. Kumar, J.W. Bullard, N. Neithalath, G. Sant, The filler effect: the influence of filler content and surface area on cementitious reaction rates, J. Amer. Ceram. Soc. 96 (2013) 1978–1990.
[71] B.K. Marsh, R.L. Day, D.G. Bonner, Strength gain and calcium hydroxide depletion in hardened cement pastes containing fly ash, Mag. Concr. Res. 38 (1986) 23–29.
[72] S. Diamond, Q. Sheng, J. Olek, Evidence of minimal pozzolanic reaction in a fly ash cement during the period of major strength development, Mater. Res. Soc. Symp. Proc. 137 (1989) 437–446.
[73] R.F. Feldman, G.G. Carette, V.M. Malhotra, Studies on mechanism of development of physical and mechanical properties of high volume fly ash-cement pastes, Cem. Concr. Comp. 12 (1990) 245–251.
[74] R. Hardtl, The pozzolanic reaction of fly ash in connection with different types of cement, Proc. 10th Int. Cong. Chem. Cem., Gothenburg, vol. 3 1997, p. 3ii082 (8pp.).
[75] V.G. Papadakis, Effect of fly ash on Portland cement systems Part I. Low-calcium fly ash, Cem. Concr. Res. 29 (1999) 1727–1736.
[76] L. Lam, W.L. Wong, C.S. Poon, Degree of hydration and gel/space ratio of high-volume fly ash/cement systems, Cem. Concr. Res. 30 (2000) 747–756.
[77] Y.M. Zhang, W. Sun, H.D. Yan, Hydration of high-volume fly ash cement pastes, Cem. Concr. Comp. 22 (2000) 445–452.
[78] S. Hanehara, F. Tomosawa, M. Kobayakawa, K. Hwang, Effects of water/powder ratio, mixing ratio of fly ash, and curing temperature on pozzolanic reaction of fly ash in cement paste, Cem. Concr. Res. 31 (2001) 31–39.
[79] K. Luke, Pulverized fuel ash as a cement extenderChpt.14 in: P. Barnes, J. Bensted (Eds.), Structure and Performance of cement, Spon Press, London, 2002.
[80] E. Sakai, S. Miyahara, S. Ohsawa, S.-H. Lee, M. Daimon, Hydration of fly ash cement, Cem. Concr. Res. 35 (2005) 1135–1140.
[81] K. De Weerdt, M. Ben Haha, G. Le Saout, K.O. Kjellsen, H. Justnes, B. Lothenbach, Hydration mechanisms of ternary Portland cements containing limestone powder and fly ash, Cem. Concr. Res. 41 (2011) 279–291.
[82] Q. Zeng, K. Li, T. Fen-chong, P. Dangla, Determination of cement hydration and pozzolanic reaction extents for fly-ash cement pastes, Constr. Build. Mater. 27 (2012) 560–569.
[83] W. Fajun, M.W. Grutzeck, D.M. Roy, The retarding effects of fly ash upon the hydration of cement pastes: the first 24 hours, Cem. Concr. Res. 15 (1985) 174–184.
[84] Concrete Society, The use of GGBS and PFA in concrete, Report of a Concrete Society Working Party, Technical Report no. 40 1991, p. TR040.
[85] J.G. Cabrera, C. Plowman, The influence of pulverised fuel ash on the early and long term strength of concrete, Proc. 7th Int. Cong. Chem. Cem., III 1980, pp. IV-84–IV-92.
[86] C. Plowman, J.G. Cabrera, The influence of pulverised fuel ash on the hydration reactions of calcium aluminates, Proc. Mater. Res. Soc. Symp. Effects of Flyash Incorporation in Cement and Concrete 1981, pp. 71–81.
[87] H. Uchikawa, S. Uchida, Influence of pozzolana on the hydration of C_3A, Proc. 7th Int. Cong. Chem. Cem., III 1980, pp. IV-24–IV-29.
[88] K. Ogawa, H. Uchikawa, K. Takemoto, The mechanism of the hydration in the system C_3S-pozzolana, Cem. Concr. Res. 10 (1980) 683–696.
[89] I. Jawed, J. Skalny, Hydration of tricalcium silicate in the presence of fly ash, Mater. res. Soc. proc. symp. effects of fly Ash Incorporation in cement and concrete, Materials Research Society, Boston November 16–18 1981, pp. 60–70.
[90] Y. Halse, D.J. Goult, P.L. Pratt, Calorimetry and microscopy of flyash and silica fume cement blends, Br. Ceram. Proc. 35 (1984) 403–417.
[91] A. Ghose, P.L. Pratt, Studies of the hydration reactions and microstructure of cement-flyash pastes, Proc. Mater. Res. Soc. Symp. Effects of Flyash Incorporation in Cement and Concrete, Materials Research Society, Boston November 16–18 1981, pp. 82–91.
[92] F. Deschner, F. Winnefeld, B. Lothenbach, S. Seufert, P. Schwesig, S. Dittrich, F. Goetz-Neunhoeffer, J. Neubauer, Hydration of Portland cement with high replacement by siliceous fly ash, Cem. Concr. Res. 42 (2012) 1389–1400.
[93] S. Abdul-Maula, I. Odler, Hydration reactions in flyash-Portland cements, proc. Mater. res. Soc. symp. effects of flyash incorporation in cement and concrete, Materials Research Society, Boston November 16–18 1981, pp. 102–111.
[94] E.E. Berry, R.T. Hemmings, W.S. Langley, G.G. Carette, Beneficated fly ash: hydration, microstructure, and strength development in Portland cement systems, Proc. 3rd Int. Conf. Fly Ash, Silica Fume, Slag, and Natural Pozzolans in Concrete, Trondheim, ACI SP-114, vol. 1 1989, pp. 241–273.
[95] H. Uchikawa, S. Uchida, S. Hanehara, Flocculation structure of fresh cement paste determined by sample freezing–back scattered electron image, Il Cemento 84 (1987) 3–22.
[96] K. Takemoto, H. Uchikawa, Hydration of pozzolanic cement, Proc. 7th Int. Cong. Chem. Cem., 1, 1980 (IV-2/1–IV-2/29).
[97] I.G. Richardson, The calcium silicate hydrates, Cem. Concr. Res. 38 (2008) 137–158.
[98] A.V. Girão, I.G. Richardson, C.B. Porteneuve, R.M.D. Brydson, Composition, morphology and nanostructure of C–S–H in white Portland cement pastes hydrated at 55 °C, Cem. Concr. Res. 37 (2007) 1571–1582.
[99] E. L'Hôpital, B. Lothenbach, G. Le Saout, D. Kulik, K. Scrivener, Incorporation of aluminium in calcium-silicate-hydrates, Cem. Concr. Res. 75 (2015) 91–103.
[100] E. Lippmaa, M. Mägi, A. Samoson, G. Engelhardt, A.R. Grimmer, Structural studies of silicates by solid-state high resolution ^{29}Si NMR, J. Am. Chem. Soc. 102 (1980) 4889–4893.
[101] E. Lippmaa, M. Mägi, M. Tarmak, W. Wieker, A.R. Grimmer, A high resolution ^{29}Si NMR study of the hydration of tricalcium silicate, Cem. Concr. Res. 12 (1982) 597–602.
[102] N.J. Clayden, C.M. Dobson, C.J. Hayes, S.A. Rodger, Hydration of tricalcium silicate followed by solid-state 29Si NMR spectroscopy, J. Chem. Soc. Cem. Commun. 1396–1397 (1984).
[103] N.J. Clayden, C.M. Dobson, G.W. Groves, S.A. Rodger, The application of solid-state nuclear magnetic resonance spectroscopy techniques to the study of the hydration of tricalcium silicate, Proc. 8th Int. Cong. Chem. Cem., III 1986, pp. 51–56.
[104] S.A. Rodger, G.W. Groves, N.J. Clayden, C.M. Dobson, A study of tricalcium silicate hydration from very early to very late stages, Mat. Res. Soc. Symp. Proc. 85 (1987) 13–20.
[105] S.A. Rodger, G.W. Groves, N.J. Clayden, C.M. Dobson, Hydration of tricalcium silicate followed by ^{29}Si NMR with cross-polarization, J. Am. Ceram. Soc. 71 (1988) 91–96.
[106] I.F. Sáez del Bosque, S. Martínez-Ramírez, M. Martín-Pastor, M.T. Blanco-Varela, Effect of temperature on C–S–H gel nanostructure in white cement, Mater. Struct. 47 (2014) 1867–1878.
[107] A.R. Brough, I.G. Richardson, G.W. Groves, C.M. Dobson, Alkali activation of reactive silicas in cements: In situ ^{29}Si MAS NMR studies of the kinetics of silicate polymerization, J. Mater. Sci. 31 (1996) 3365–3373.

[108] J. Hjorth, J. Skibsted, H.J. Jakobsen, ^{29}Si MAS NMR studies of Portland cement components and effects of microsilica on the hydration reaction, Cem. Concr. Res. 18 (1988) 789–798.
[109] G. Parry-Jones, A.J. Al-Tayyib, S.U. Al-Dulaijan, A.I. Al-Mana, ^{29}Si MAS-NMR hydration and compressive strength study in cement, Cem. Concr. Res. 19 (1989) 228–234.
[110] S.U. Al-Dulaijan, G. Parry-Jones, A.J. Al-Tayyib, A.I. Al-Mana, ^{29}Si magic-angle-spinning nuclear magnetic resonance study of hydrated cement paste and mortar, J. Am. Ceram. Soc. 3 (1990) 736–739.
[111] X. Cong, R.J. Kirkpatrick, ^{17}O and ^{29}Si MAS NMR study of β-C_2S hydration and the structure of calcium-silicate hydrates, Cem. Concr. Res. 23 (1993) 1065–1077.
[112] A.R. Brough, C.M. Dobson, I.G. Richardson, G.W. Groves, In situ solid state NMR studies of Ca_3SiO_5: hydration at room temperature and at elevated temperatures using ^{29}Si enrichment, J. Mater. Sci. 29 (1994) 3926–3940.
[113] I.G. Richardson, G.W. Groves, S.A. Rodger, The porosity and pore structure of hydrated cement pastes as revealed by electron microscopy techniques, Mater. Res. Soc. Symp. Proc. 137 (1989) 313–318.
[114] S.A. Rodger, G.W. Groves, The microstructure of tricalcium silicate/pulverized-fuel ash blended cement pastes, Adv. Cem. Res. 1 (1988) 84–91.
[115] S.A. Rodger, G.W. Groves, Electron microscopy study of ordinary Portland cement and ordinary Portland cement–pulverised fuel ash blended pastes, J. Am. Ceram. Soc. 72 (1989) 1037–1039.
[116] H.S. Pietersen, Application of TEM to characterize fly and slag cements, Heron 44 (1999) 299–312.
[117] D. Kulik, Improving the structural consistency of C-S-H solid solution thermodynamic models, Cem. Concr. Res. 41 (2011) 477–495.
[118] R.J. Myers, S.A. Bernal, J.L. Provis, A thermodynamic model for C-(N-)A-S-H gel: CNASH_ss. Derivation and validation, Cem. Concr. Res. 66 (2014) 27–47.
[119] E.T. Rodriguez, I.G. Richardson, L. Black, E. Boehm-Courjault, A. Nonat, J. Skibsted, Composition, Silicate Anion Structure and Morphology of Calcium Silicate Hydrates (C-S-H) Synthesized by Silica-Lime Reaction and by the Controlled Hydration of Tricalcium Silicate (C_3S)(Accepted for publication in) Adv. App. Ceram. (2015), http://dx.doi.org/10.1080/17436753.2015.1122330.
[120] H. Bassett, Notes on the system lime-water, and on the determination of calcium, J. Chem. Soc. 1270–1275 (1934).
[121] J. Johnston, C. Grove, The solubility of calcium hydroxide in aqueous salt solutions, J. Am. Chem. Soc. 53 (1931) 3976–3991.
[122] R.G. Bates, V.E. Bower, E.R. Smith, Calcium hydroxide as a highly alkaline pH standard, J. Res. Natl. Bur. Stand. 56 (1956) 305–312.
[123] J. Duchesne, E.J. Reardon, Measurement and prediction of portlandite solubility in alkali solutions, Cem. Concr. Res. 25 (1995) 1043–1053.
[124] P. Longuet, L. Burglen, A. Zelwer, The liquid phase of hydrated cement, Rev. Mater. Constr. 676 (1973) 35–41 (in French).
[125] R.S. Barneyback, S. Diamond, Expression and analysis of pore fluids from hardened cement pastes and mortars, Cem. Concr. Res. 11 (1981) 279–285.
[126] F.P. Glasser, K. Luke, M.J. Angus, Modification of cement pore fluid compositions by pozzolanic additives, Cem. Concr. Res. 18 (1988) 165–178.
[127] D. Constantiner, D. Diamond, in: K.L. Scrivener, J.F. Young, E & FN Spon (Eds.),Pore solution analysis: Are there pressure effects?, Proc. Mater. Res. Soc. Symp. on Mechanisms of Chemical Degradation of Cement-Based Systems 1997, pp. 22–29.
[128] J. Duchesne, M.A. Berube, Evaluation of the validity of the pore solution expression method from hardened cement pastes and mortars, Cem. Concr. Res. 24 (1994) 456–462.
[129] B. Lothenbach, Thermodynamic equilibrium calculations in cementitious systems, Mater. Struct. 43 (2010) 1413–1433.
[130] V.A. Lashchenko, V.I. Loganina, Liquid phase of hydrated Portland cement, Zh. Prikl. Khim. 47 (1974) 645–647 (in Russian).
[131] S. Diamond, Effects of two Danish flyashes on alkali contents of pore solutions of cement-flyash pastes, Cem. Concr. Res. 11 (1981) 383–394.
[132] C.L. Page, Ø. Vennesland, Pore solution composition and chloride binding capacity of silica-fume cement pastes, Mater. Constr. 16 (1983) 19–25.
[133] J.-G. Xue, W.-X. Xu, M.-X. Ye, A study of the liquid phase separated from the pores of hardened cement paste, Kuei Suan Yen Hsueh Pao (J. Chin. Silic. Soc.) 11 (1983) 276–289.
[134] F.P. Glasser, J. Marr, The alkali binding potential of OPC and blended cements, Il Cemento 82 (1985) 85–94.
[135] M. Silsbee, R.I.A. Malek, D.M. Roy, Composition of the pore fluids extruded from slag-cement pastes, Proc. 8th Int. Cong. Chem. Cem., IV 1986, pp. 263–269.
[136] I. Canham, C.L. Page, P.J. Nixon, Aspects of the pore solution chemistry of blended cements related to the control of alkali silica reaction, Cem. Concr. Res. 17 (1987) 839–844.
[137] K. Andersson, B. Allard, M. Bengtsson, B. Magnusson, Chemical composition of cement pore solutions, Cem. Concr. Res. 19 (1989) 327–332.
[138] A.L.A. Fraay, J.M. Bijen, Y.M. de Haan, The reaction of fly ash in concrete, Cem. Concr. Res. 19 (1989) 235–246.
[139] S. Goñi, M.P. Lorenzo, A. Guerrero, M.S. Hernández, Calcium hydroxide saturation factors in the pore solution of hydrated Portland cement fly ash pastes, J. Am. Ceram. Soc. 79 (1996) 1041–1046.
[140] E.E. Lachowski, F.P. Glasser, A. Kindness, K. Luke, Compositional development (solid and aqueous phase) in aged slag and fly ash blended cement pastes, Proc. 10th Int. Cong. Chem. Cem., Gothenburg 1997, p. 3ii091 (8 pp.).
[141] M.H. Shehata, M.D.A. Thomas, R.F. Bleszynski, The effects of fly ash composition on the chemistry of pore solution in hydrated cement pastes, Cem. Concr. Res. 29 (1999) 1915–1920.
[142] S. Song, H.M. Jennings, Pore solution chemistry of alkali-activated ground granulated blast-furnace slag, Cem. Concr. Res. 29 (1999) 159–170.
[143] S. Song, D. Sohn, H.M. Jennings, T.O. Mason, Hydration of alkali-activated ground granulated blast furnace slag, J. Mater. Sci. 35 (2000) 249–257.
[144] J.K. Tishmack, J. Olek, S. Diamond, S. Sahu, Characterization of pore solutions expressed from high-calcium fly-ash–water pastes, Fuel 80 (2001) 815–819.
[145] D. Rothstein, J.J. Thomas, B.J. Christensen, H.M. Jennings, Solubility behavior of Ca-, S-, Al-, and Si-bearing solid phases in Portland cement pore solutions as a function of hydration time, Cem. Concr. Res. 32 (2002) 1663–1671.
[146] F. Puertas, A. Fernández-Jiménez, M.T. Blanco-Varela, Pore solution in alkali-activated slag cement pastes. Relation to the composition and structure of calcium silicate hydrate, Cem. Concr. Res. 34 (2004) 139–148.
[147] B. Lothenbach, F. Winnefeld, C. Alder, E. Wieland, P. Lunk, Effect of temperature on the pore solution, microstructure and hydration products of Portland cement pastes, Cem. Concr. Res. 37 (2007) 483–491.
[148] K. Luke, E. Lachowski, Internal composition of 20-year-old fly ash and slag-blended ordinary Portland cement pastes, J. Am. Ceram. Soc. 91 (2008) 4084–4092.
[149] B. Lothenbach, F. Winnefeld, Thermodynamic modelling of the hydration of Portland cement, Cem. Concr. Res. 36 (2006) 209–226.
[150] A. Kumar, G. Sant, C. Patapy, C. Gianocca, K.L. Scrivener, The influence of sodium and potassium hydroxide on alite hydration: experiments and simulations, Cem. Concr. Res. 42 (2012) 1513–1523.
[151] E.J. Reardon, Problems and approaches to the prediction of the chemical composition in cement-water systems, Waste Manag. 12 (1992) 221–239.
[152] F.P. Glasser, J. Pedersen, K. Goldthorpe, M. Atkins, Solubility reactions of cement components with NaCl solutions: I. $Ca(OH)_2$ and C-S-H, Adv. Cem. Res. 17 (2005) 57–64.
[153] J.J. Thomas, D. Rothstein, H.M. Jennings, B.J. Christensen, Effect of hydration temperature on the solubility behavior of Ca-, S-, Al-, and Si-bearing solid phases in Portland cement pastes, Cem. Concr. Res. 33 (2003) 2037–2047.
[154] E. Gallucci, P. Mathur, K.L. Scrivener, Microstructural development of early age hydration shells around cement grains, Cem. Concr. Res. 40 (2010) 4–13.
[155] E.M. Gartner, K.E. Kurtis, P.J.M. Monteiro, Proposed mechanism of C-S-H growth tested by soft X-ray microscopy, Cem. Concr. Res. 30 (2000) 817–822.
[156] M.C.G. Juenger, V.H.R. Lamour, P.J.M. Monteiro, E.M. Gartner, G.P. Denbeaux, Direct observation of cement hydration by soft X-ray transmission microscopy, J. Mat. Sci. Lett. 22 (2003) 1335–1337.
[157] M.C.G. Juenger, P.J.M. Monteiro, E.M. Gartner, G.P. Denbeaux, A soft X-ray microscope investigation into the effects of calcium chloride on tricalcium silicate hydration, Cem. Concr. Res. 35 (2005) 19–25.
[158] A.R. Brough, C.M. Dobson, I.G. Richardson, G.W. Groves, A study of the pozzolanic reaction by solid-state ^{29}Si NMR using selective isotopic enrichment, J. Mater. Sci. 30 (1995) 1671–1678.